

**AERODYNAMIC CHARACTERISTICS OF PERFORATED  
WALLS FOR TRANSONIC WIND TUNNELS**



**PROPULSION WIND TUNNEL FACILITY  
ARNOLD ENGINEERING DEVELOPMENT CENTER  
AIR FORCE SYSTEMS COMMAND  
ARNOLD AIR FORCE STATION, TENNESSEE 37389**

**June 1977**

**Final Report for Period January 1, 1975 - January 1, 1977**

Approved for public release; distribution unlimited.

**Prepared for**

**DIRECTORATE OF TECHNOLOGY  
ARNOLD ENGINEERING DEVELOPMENT CENTER  
AIR FORCE SYSTEMS COMMAND  
ARNOLD AIR FORCE STATION, TENNESSEE 37389**

## NOTICES

When U. S. Government drawings specifications, or other data are used for any purpose other than a definitely related Government procurement operation, the Government thereby incurs no responsibility nor any obligation whatsoever, and the fact that the Government may have formulated, furnished, or in any way supplied the said drawings, specifications, or other data, is not to be regarded by implication or otherwise, or in any manner licensing the holder or any other person or corporation, or conveying any rights or permission to manufacture, use, or sell any patented invention that may in any way be related thereto.

Qualified users may obtain copies of this report from the Defense Documentation Center.

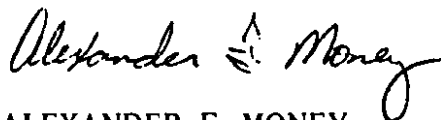
References to named commercial products in this report are not to be considered in any sense as an endorsement of the product by the United States Air Force or the Government.

This report has been reviewed by the Information Office (OI) and is releasable to the National Technical Information Service (NTIS). At NTIS, it will be available to the general public, including foreign nations.

## APPROVAL STATEMENT

This technical report has been reviewed and is approved for publication.

FOR THE COMMANDER



ALEXANDER F. MONEY  
Research and Development  
Division  
Directorate of Technology



ROBERT O. DIETZ  
Director of Technology

# UNCLASSIFIED

REPORT DOCUMENTATION PAGE		READ INSTRUCTIONS BEFORE COMPLETING FORM
1. REPORT NUMBER <b>AEDC-TR-77-61</b>	2. GOVT ACCESSION NO.	3. RECIPIENT'S CATALOG NUMBER
4. TITLE (and Subtitle) <b>AERODYNAMIC CHARACTERISTICS OF PERFORATED WALLS FOR TRANSONIC WIND TUNNELS</b>		5. TYPE OF REPORT & PERIOD COVERED <b>Final Report - January 1, 1975- January 1, 1977</b>
		6. PERFORMING ORG. REPORT NUMBER
7. AUTHOR(s) <b>J. L. Jacocks, ARO, Inc.</b>		8. CONTRACT OR GRANT NUMBER(s)
9. PERFORMING ORGANIZATION NAME AND ADDRESS <b>Arnold Engineering Development Center (DY) Air Force Systems Command Arnold Air Force Station, Tennessee 37389</b>		10. PROGRAM ELEMENT, PROJECT, TASK AREA & WORK UNIT NUMBERS <b>Program Element 65807F</b>
11. CONTROLLING OFFICE NAME AND ADDRESS <b>Arnold Engineering Development Center (DYFS) Air Force Systems Command Arnold Air Force Station, Tennessee 37389</b>		12. REPORT DATE <b>June 1977</b>
		13. NUMBER OF PAGES <b>75</b>
14. MONITORING AGENCY NAME & ADDRESS (if different from Controlling Office)		15. SECURITY CLASS. (of this report) <b>UNCLASSIFIED</b>
		15a. DECLASSIFICATION/DOWNGRADING SCHEDULE <b>N/A</b>
16. DISTRIBUTION STATEMENT (of this Report)  <b>Approved for public release; distribution unlimited.</b>		
17. DISTRIBUTION STATEMENT (of the abstract entered in Block 20, if different from Report)		
18. SUPPLEMENTARY NOTES  <b>Available in DDC</b>		
19. KEY WORDS (Continue on reverse side if necessary and identify by block number) <b>transonic wind tunnels perforation walls aerodynamic characteristics</b>		
20. ABSTRACT (Continue on reverse side if necessary and identify by block number) <b>A combined experimental-theoretical approach is developed for determination of the crossflow characteristics of ventilated walls. The technique is based on measurement of static pressures at the boundaries of a two-dimensional flow, calculation of the interior flow properties with Murman-Cole type finite difference techniques, and calculation of the boundary-layer development on and mass flux distribution through the ventilated wall using Patankar-Spalding type solution techniques. Results verify the validity</b>		

## UNCLASSIFIED

# UNCLASSIFIED

## 20. ABSTRACT (Continued)

of assuming proportionality between local pressure and flow angle as a boundary condition for wall interference estimates. However, it is also shown that the thickness of the boundary layer represents a dominant influence on the perforated wall characteristics, with both the slope and intercept of the characteristic being dependent on the boundary layer. The effects on the wall characteristics of suppressing the edgetone noise by use of screen overlays or splitter plates within discrete holes are documented.

Approved for  
to be published  
Distribution  
of this  
report  
is unlimited

## PREFACE

The work reported herein was conducted by the Arnold Engineering Development Center (AEDC), Air Force Systems Command (AFSC), under Program Element 65807F. The results were obtained by ARO, Inc., AEDC Division (a Sverdrup Corporation Company), operating contractor for the AEDC, AFSC, Arnold Air Force Station, Tennessee, under ARO Project Numbers P32A-29A, P32A-COA, and P32A-J5A. The author of this report was J. L. Jacocks, ARO, Inc. The manuscript (ARO Control No. ARO-PWT-TR-77-30) was submitted for publication on April 25, 1977.

## CONTENTS

	<u>Page</u>
1.0 INTRODUCTION . . . . .	5
2.0 DEVELOPMENT OF THEORY	
2.1 Potential Flow . . . . .	6
2.2 Wall Boundary Layer . . . . .	14
3.0 APPARATUS	
3.1 Aerodynamic Wind Tunnel (1T) . . . . .	17
3.2 Pressure Disturbance Generators . . . . .	18
3.3 Perforated Wall Geometry . . . . .	21
3.4 Instrumentation . . . . .	21
4.0 PROCEDURE	
4.1 Test Procedure . . . . .	26
4.2 Precision of Measurements . . . . .	27
5.0 RESULTS AND DISCUSSION	
5.1 Assessment of Accuracy . . . . .	27
5.2 Perforated Wall Characteristics . . . . .	30
5.3 Effect of Noise Suppression Devices . . . . .	43
6.0 CONCLUDING REMARKS . . . . .	48
REFERENCES . . . . .	50

## ILLUSTRATIONS

### Figure

1. Schematic of Physical Model and Corresponding Math Model . . . . .	7
2. Comparison of the Inverse Small-Perturbation Approach with an Exact Solution for Flow over a Right-Circular Cylinder . . . . .	11
3. Comparison of the Inverse Small-Perturbation Approach with Exact Solutions for Flow Through Oblique Shocks . . . . .	13
4. Illustration of the Nonlinear Relationship Between Flow Angle and Normalized Wall Mass Flux . . . . .	16

<u>Figure</u>	<u>Page</u>
5. Characteristics of the Pressure Disturbance Generators . . . . .	19
6. Perforated Wall Geometry . . . . .	22
7. Comparison of Calculated Flow Angle Distributions with Laser Velocimetry Measurement . . . . .	29
8. Comparison of Calculated and Measured Boundary-Layer Displacement Thickness . . . . .	31
9. Representative Variation of Pressure Coefficient, Flow Inclination, Wall Mass Flux, and Boundary-Layer Displacement Thickness with Tunnel Station . . . . .	32
10. Representative Locus of Pressure Coefficient and Flow Inclination - the Wall Characteristic . . . . .	34
11. Variability of the Wall Characteristic with Changes in the Imposed Pressure Distribution . . . . .	36
12. Effect of Boundary-Layer Displacement Thickness on the Characteristic Slope . . . . .	37
13. Effect of Boundary-Layer Displacement Thickness on the Characteristic Intercept . . . . .	40
14. Comparison of the Variable-Porosity Wall Characteristics for Upstream and Downstream Displacement of the Cutoff Plate . . . . .	42
15. Effect of Noise Suppression Devices on the Characteristics of Configuration A . . . . .	44
16. Effect of Noise Suppression Devices on the Char- acteristics of Configuration D . . . . .	46

**APPENDIX**

A. COMPARATIVE CROSSFLOW CHARACTERISTIC DATA FOR EACH PERFORATED WALL GEOMETRY . . . . .	53
NOMENCLATURE . . . . .	74

## 1.0 INTRODUCTION

Although transonic wind tunnels with ventilated test section walls have been in use for over 25 years (Ref. 1), an understanding of the aerodynamic properties of the walls has yet to be developed. Knowledge of the wall crossflow characteristics (pressure-flow angle relationship) is required for several reasons, but an accurate method has not been available to obtain this information. Previous techniques (Refs. 1 through 3) for determination of wall characteristics have relied on the assumption of equivalence between flow angle at the wall and mass flux through the wall. However, Rae (as reported in Ref. 4) demonstrated that the boundary-layer development on the wall created a nonlinear interdependence between mass flux and flow angle.

Direct measurement of the local static pressure and flow angle in the vicinity of a ventilated wall can be accomplished, as shown by Berndt (Ref. 5). This approach is feasible for documentation of the characteristics of a given wall geometry, but becomes inefficient as the number of wall configurations is increased.

To bypass these difficulties, the present investigation was designed to develop a new test technique that would yield definitive information on ventilated wall characteristics. An inverse technique was selected wherein sufficient yet tractable static pressure measurements made at the boundaries of a two-dimensional flow would allow calculation of the remaining flow variables. The potential flow field was calculated with the line relaxation method of Murman and Cole (Ref. 6) with the primary result being the flow angle distribution in the vicinity of a ventilated wall. The measured pressures and inferred flow angles were then used to calculate the boundary-layer development on and mass-flux distribution through the ventilated wall.

The theoretical approach is described in Section 2.0, with the experimental apparatus and procedure being described in Sections 3.0 and 4.0. Section 5.0 presents the results, including independent measurements made to verify the accuracy of the theoretical calculations.

## 2.0 DEVELOPMENT OF THEORY

### 2.1 POTENTIAL FLOW

The basic hypothesis of the present work is presented pictorially in Fig. 1. It is assumed that a two-dimensional transonic flow field can be established within a region bounded by a contoured solid (bottom) wall, solid plane sidewalls, and a ventilated (top) wall. It is further assumed that the flow can be mathematically described by small perturbations from a uniform flow with boundary conditions derived from static pressure measurements around a control volume. The line relaxation technique of Murman and Cole (Ref. 6) provides the calculational tool to solve the resulting boundary-value problem. The result is the distribution of flow angle in the vicinity of the ventilated wall.

The small perturbation, two-dimensional, potential flow equation descriptive of internal transonic flow is given (Ref. 7) by

$$\left[ 1 - M^2 - (\gamma + 1)M^2 \phi_x \right] \phi_{xx} + \phi_{yy} = 0 \quad (1)$$

where  $\phi_x$  and  $\phi_y$  are the perturbation velocities (divided by a reference velocity) parallel and normal to the tunnel axis and  $M$  is a reference Mach number. To the degree of approximation inherent within Eq. (1) the local pressure coefficient,  $C_p$ , and flow angle,  $\theta$ , are given by

$$C_p = -2 \phi_x \quad (2)$$

$$\theta = \phi_y$$

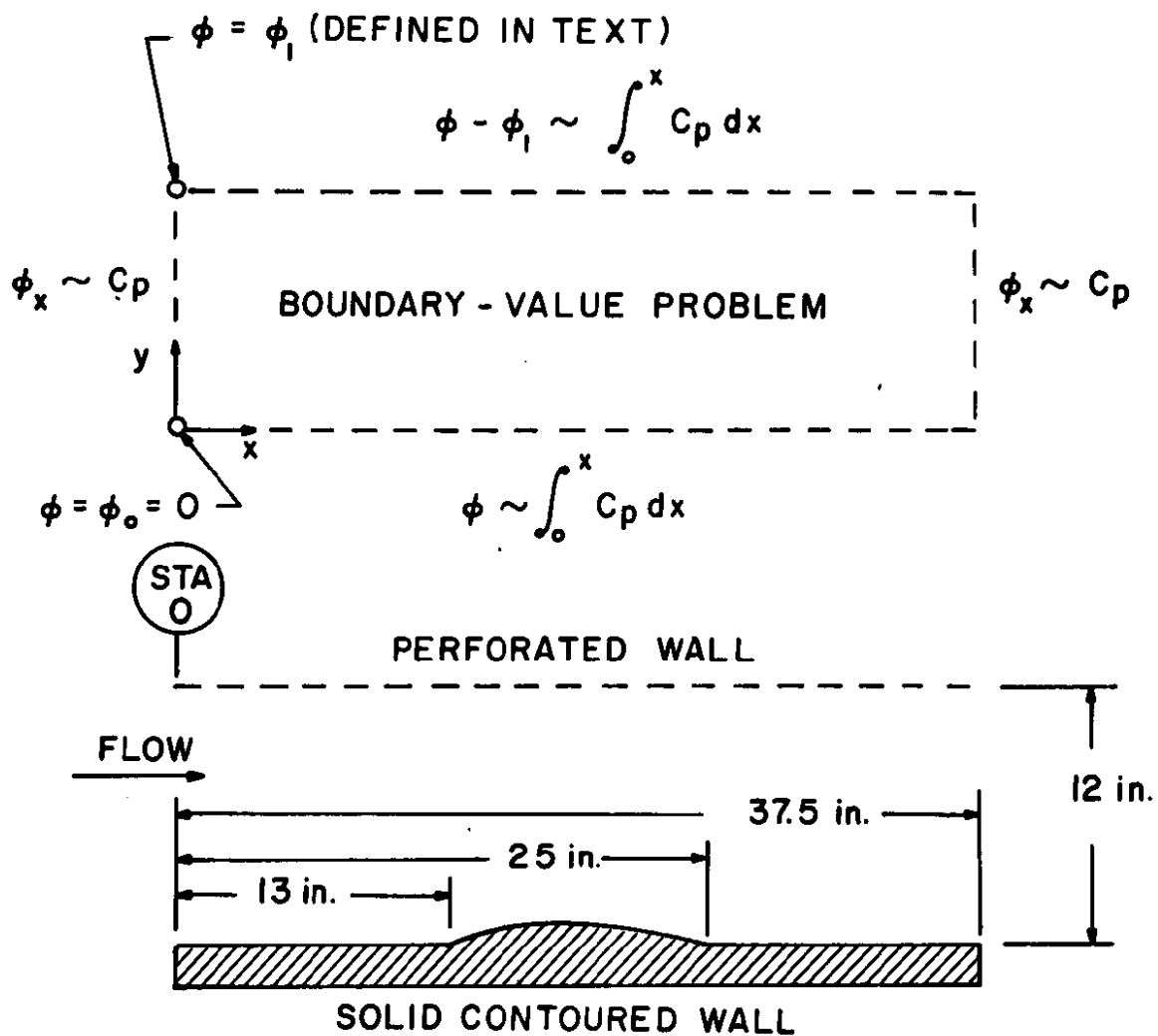


Figure 1. Schematic of physical model and corresponding math model.

Measurements of static pressure at the boundaries of a control volume as indicated in Fig. 1 can be used to specify sufficient boundary conditions of mixed type to obtain a solution of Eq. (1). Specifically, natural boundary conditions at the upstream and downstream planes of the control volume are given by

$$\begin{aligned}\phi_x(o,y) &= -0.5 C_p(o,y) \\ \phi_x(L,y) &= -0.5 C_p(L,y)\end{aligned}\quad (3)$$

Boundary conditions of the Dirichlet type are obtained by integration of the measured pressures at the top and bottom boundaries by

$$\begin{aligned}\phi(x,o) &= -0.5 \int_0^x C_p(x,o) dx + \phi_o \\ \phi(x,h) &= -0.5 \int_0^x C_p(x,h) dx + \phi_1\end{aligned}\quad (4)$$

where two constants of integration ( $\phi_o$  and  $\phi_1$ ) remain to be evaluated. A physical interpretation of the significance of these constants is that their difference represents the average flow inclination at the upstream boundary of the test section, or

$$\phi_1 - \phi_o = \int_0^h \phi_y(o,y) dy \quad (5)$$

Since the magnitude of the potential is of no consequence,  $\phi_o$  was arbitrarily set to zero without loss of generality. The remaining constant of integration cannot be evaluated from the static pressure measurements alone but requires an additional item of information relating to flow inclination or geometry.

The selected procedure for defining  $\phi_1$  was based on the concept of boundary-layer displacement thickness development on the bottom wall with, of course, knowledge of the wall geometry. For each flow condition, a preliminary solution of the flow field compatible with the

measured pressures was numerically obtained assuming  $\phi_1 = 0$ , say  $\hat{\phi}(x,y)$ . The elevation,  $y_s$ , of the streamline through the coordinate origin was then computed from numerical differentiation and integration of this solution in the form of

$$y_s(x) = \int_0^x \hat{\phi}_y(x,0) dx \quad (6)$$

In general, the resulting streamline did not agree with the effective wall geometry because the average flow inclination at the test section entrance cannot be assumed a priori. However, superposition of a uniform crossflow on the  $\hat{\phi}$  solution does allow matching of both the effective bottom wall geometry and the boundary conditions derived from static pressure measurements. The required crossflow was determined explicitly by forcing agreement between the computed streamline (with rotation) and the effective wall elevation at two points,  $x = 0$  and  $x = x_1$ . The resulting rotated streamline generally agreed with the effective geometry for all values of  $x$ , with allowance for the expected accuracy level because of the small perturbation assumption. Given the displacement thickness,  $\delta_1$ , and the wall geometry,  $y_g$ ,  $\phi_1$  was computed from

$$\phi_1 = \frac{h}{x_1} \left[ \delta_1(x_1) - \delta_1(0) + y_g(x_1) - y_s(x_1) \right] \quad (7)$$

The displacement thickness at the test section entrance,  $\delta_1(0)$ , was measured and found to be weakly dependent on Mach number and, for convenience, a nominal value of 0.07 in. was used for all calculations. During the first portion of experiments, the displacement thickness was measured at the test section exit for each flow condition and used in Eq. (7), whereas for the later experiments,  $x_1$  was fixed at the middle of the test section with  $\delta_1 = 0.04$  in., which was representative of measured values.

Superposition of the uniform crossflow does not require extensive recomputation of the flow field because Eq. (1) is linear in this respect, and the final solution is given by

$$\phi(x,y) = \hat{\phi}(x,y) + \frac{y}{h} \phi_1 \quad (8)$$

The numerical technique selected to solve for  $\hat{\phi}$  was that of Murman and Cole (Ref. 6). A computer code was written specifically for a finite control volume with boundary conditions applicable to the present problem. The finite-difference representation of Eq. (1) was coded with a mesh of uniform spacing in each of the coordinate directions. The difference operator was varied among elliptic, parabolic, hyperbolic, and a special shock-point differencing (Ref. 8) according to the local Mach number and velocity gradient. Boundary conditions were applied at the boundaries of the mesh.

Several idealized numerical experiments were conducted to verify the accuracy of the coding and the practicality of the solution. These studies included verification of stability, ability to rapidly converge with imbedded shocks, self-consistency between inverse and direct solutions, and comparisons with other exact and approximate solutions.

One of the most illustrative examples of the accuracy of the small-perturbation approach is provided by comparison with an exact solution for flow over a right-circular cylinder (Ref. 9). As indicated in Fig. 2, a control volume was selected in the vicinity of a cylinder immersed in uniform incompressible potential flow. Both the exact pressure coefficient distribution on the streamline representing the bottom wall and the distribution on the other three boundaries were used to solve for the inclusive flow field. The calculated flow angles at the upper and lower boundaries are compared with the exact solution in Fig. 2. Two salient points of this comparison are that the inverse solution appears to be nominally ten percent in error, a consequence of assuming

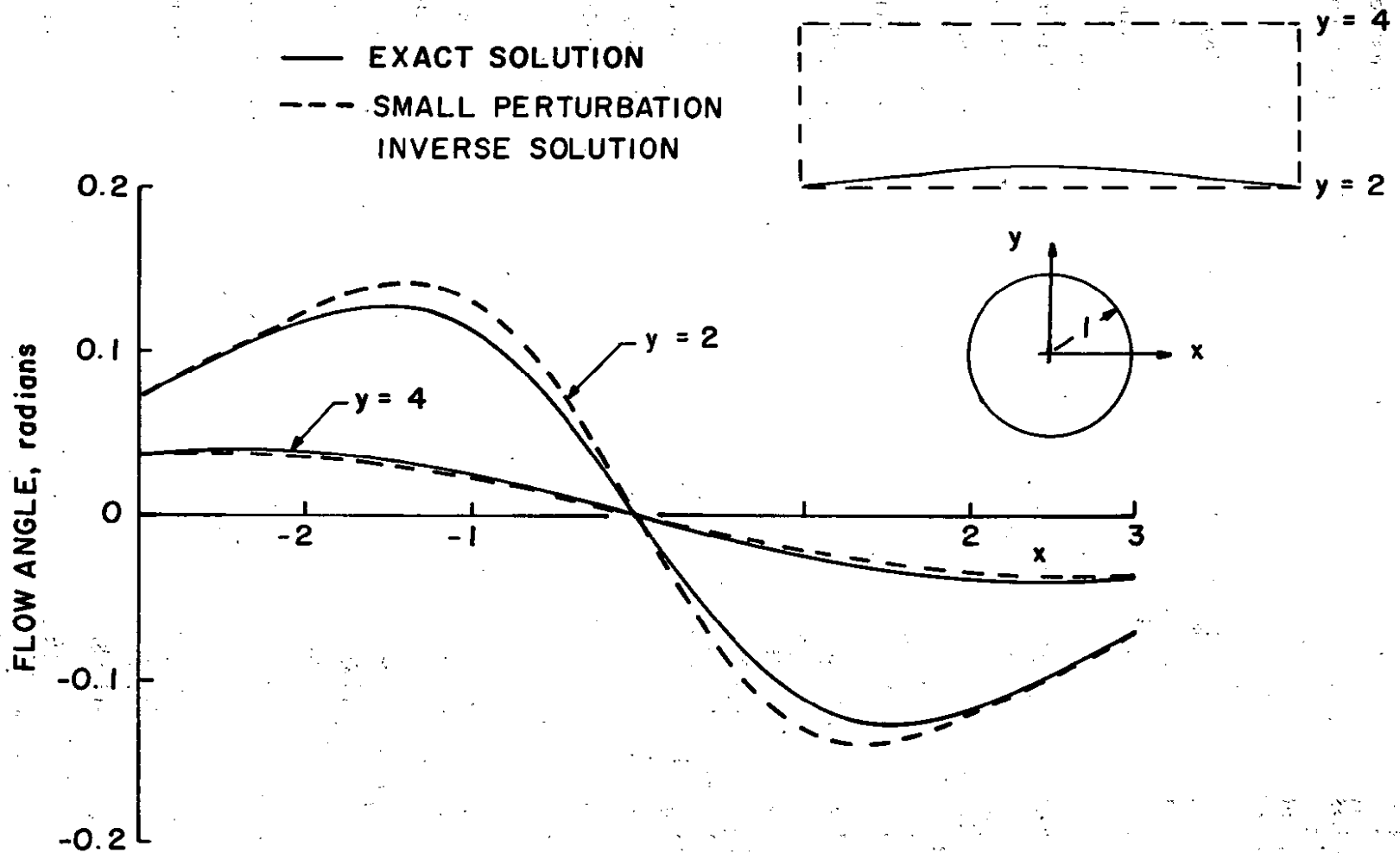


Figure 2. Comparison of the inverse small-perturbation approach with an exact solution for flow over a right-circular cylinder.

small perturbations, and that, beginning with symmetric inputs, the calculational scheme yields symmetric results. It should be noted that  $M = 0.1$  was assumed for these computations, but the nonlinear transonic characteristic of Eq. (1) was retained.

It can be argued that the use of experimentally determined (exact) pressure coefficients as boundary conditions is inconsistent with the degree of approximation implicit in Eq. (1). This hypothesis was examined by using as boundary conditions pressure coefficients computed by subtracting the higher-order velocity terms from the exact distributions. The resulting calculated flow angles were compared with the exact solution for flow over a cylinder and showed errors up to three times that indicated in Fig. 2. It was concluded that the inverse solution approach in combination with tangential rather than normal boundary conditions were in concert and would yield results compatible with the real flow.

A second class of illustrative examples of the usefulness of the technique is based on uniform flow through an oblique planar shock. In Fig. 3, two examples are given that were constructed from the exact solution to the Euler equations. In these examples, flows at Mach numbers of 1.1 and 1.2 were turned by a shock at angles of 75 and 60 deg, respectively. The major difference between the two is that the stronger shock results in subsonic flow, whereas the other flow is supersonic throughout. For the supersonic flow, backward or upstream differencing is consistently utilized; hence errors are accumulated within the field that are incompatible with the exact, imposed boundary conditions, and a reflection back into the field occurs at the boundaries. For the subsonic downstream flow, central differencing is utilized, permitting communication of the imposed boundary conditions into the field with correspondingly more accurate results. These findings were not unexpected, since it was known (Ref. 6) that the hyperbolic differencing operator was only accurate to the first-order, and second-order accuracy was characteristic of the elliptic differencing operator.

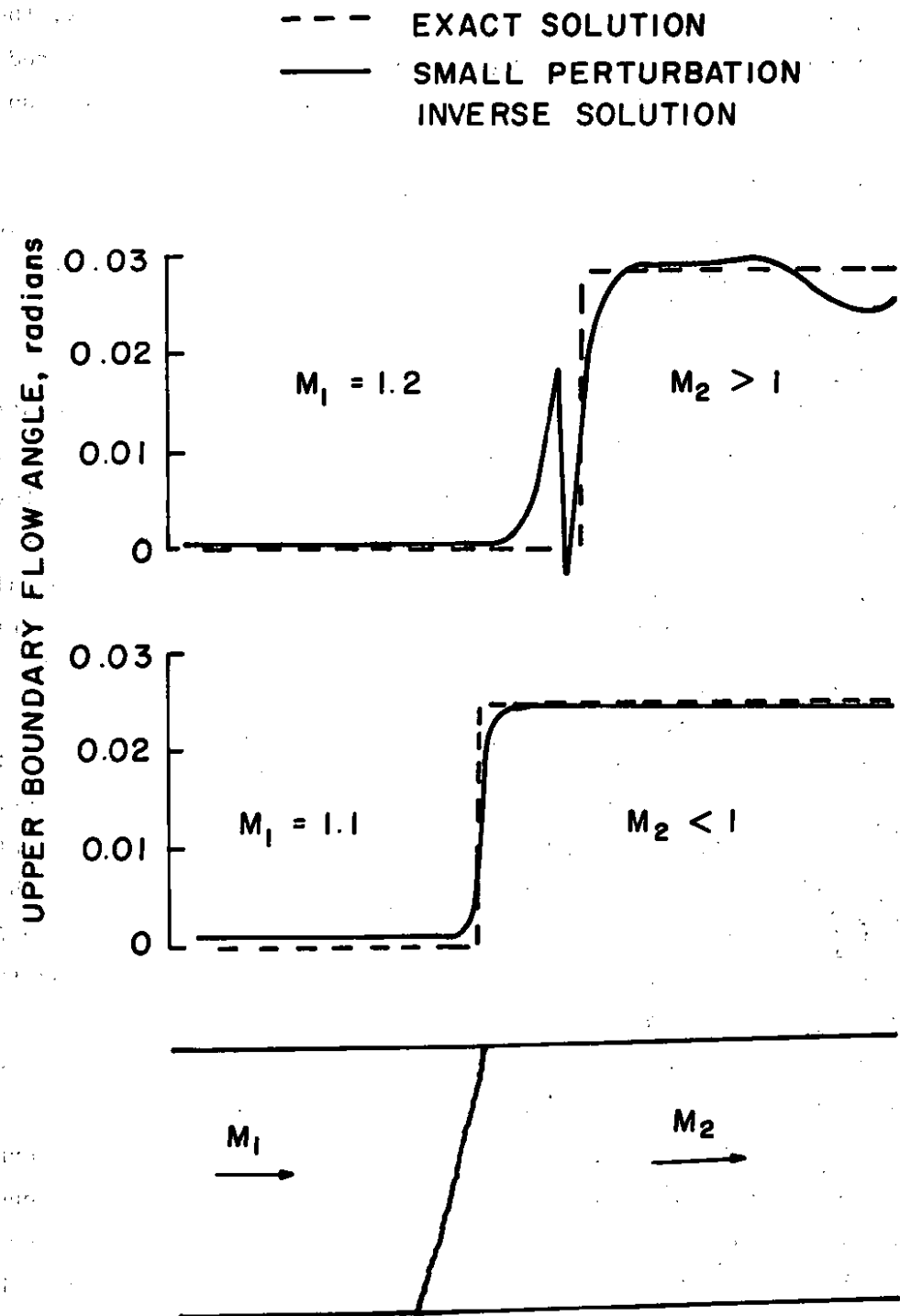


Figure 3. Comparison of the inverse small-perturbation approach with exact solutions for flow through oblique shocks.

From these numerical experiments, it was concluded that the calculated flow angles in the vicinity of a ventilated wall would be of usable accuracy for entirely subcritical flows, but that the adequacy of the procedure would require close reassessment for conditions with a large region of supercritical flow.

## 2.2 WALL BOUNDARY LAYER

As discussed by Goethert (Ref. 6) and Lukasiewicz (Ref. 10), the boundary-layer (displacement) thickness is an important parameter if correlations of ventilated wall characteristics are attempted. The presence of a boundary layer also results in a nonlinear relationship between flow inclination and wall mass flux as illustrated by Rae (Ref. 4). This effect can be readily appreciated by considering the integral continuity equation for two-dimensional flow written as

$$\frac{d\delta_1}{dx} - \frac{\delta_\infty - \delta_1}{\rho_\infty u_\infty} \frac{d}{dx} (\rho_\infty u_\infty) + \theta - \lambda = 0 \quad (9)$$

where  $\delta_1$  is the displacement thickness,  $\delta_\infty$  is a constant thickness inclusive of the boundary layer where the streamwise mass flux  $\rho_\infty u_\infty$  is evaluated,  $\theta$  the flow inclination at  $\delta_\infty$ , and  $\lambda$  is the mass flux through the wall normalized by  $\rho_\infty u_\infty$ . Note that the sign convention adopted for  $\theta$  and  $\lambda$  is such that suction (outflow) is positive. Ignoring the effects of pressure gradients, equality of  $\theta$  and  $\lambda$  would require constant displacement thickness, which generally does not occur.

The conventional approach to the calculation of boundary-layer development over a porous wall requires specification of the wall mass flux as an independent parameter. Since flow angle outside of the boundary layer was known for the present approach, a method for using Eq. (9) to solve for the mass flux was developed by G. H. Saunders of ARO, Inc. The two-dimensional, turbulent, boundary-layer prediction code of Whitfield (Ref. 11), based on that of Patankar and Spalding

(Ref. 12), was modified to incorporate the integral continuity equation to relate wall mass flux to flow angle. For each streamwise increment within the boundary-layer calculation, the wall mass flux was iteratively specified until the calculated flow angle from Eq. (9) matched the potential flow results. The end result of these calculations was the wall mass-flux distribution, boundary-layer development, and the distribution of other parameters such as skin friction and boundary-layer shape factor. The results must be interpreted with caution because, in addition to the usual boundary-layer approximations, it was implicitly assumed that the finite-size perforations could be represented as an equivalent, homogeneous porous wall and that the no-slip condition was valid (in spite of having inclined holes).

Another functional relationship between mass flux and flow angle can be derived (Ref. 4) from a combination of the integral continuity and momentum equations and is given by

$$\lambda = \frac{1}{1+H} \left\{ \theta + \delta_2 \frac{dH}{dx} + H \frac{C_f}{2} + \frac{1}{2} \frac{dC}{dx} \left[ \delta_1 (1+H) + \delta_\infty (1-M^2) \right] \right\} \quad (10)$$

The parameters of significance are the shape factor,  $H$ , and the skin-friction coefficient,  $C_f$ . For large suction, the shape factor approaches unity and the skin-friction coefficient is of comparable magnitude to the mass flux which results in  $\lambda \sim \theta$ . Conversely, for large blowing, the skin friction approaches zero and the shape factor becomes large such that  $d\lambda/d\theta \rightarrow 0$ . At moderate suction or blowing rates with a representative shape factor of  $H = 1.5$  at the Mach numbers of interest, Eq. (10) indicates  $\lambda \sim \theta/2.5$  would be appropriate. Some representative comparisons of the relationship between mass flux and flow angle as computed from Whitfield's code are presented in Fig. 4. These results are in accord with Eq. (10) and clearly illustrate the nonlinearity between flow inclination and normalized wall mass flux.

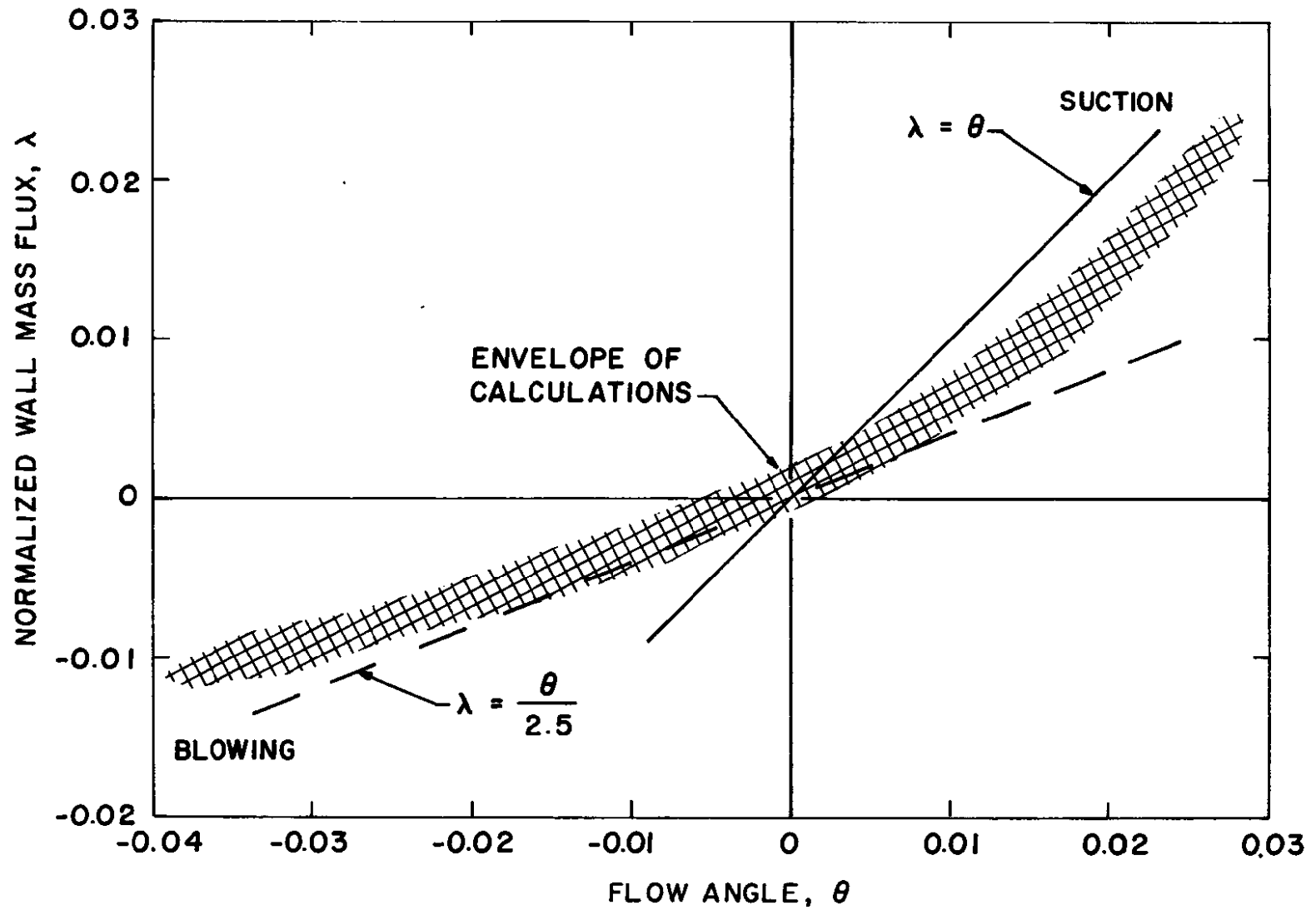


Figure 4. Illustration of the nonlinear relationship between flow angle and normalized wall mass flux.

### 3.0 APPARATUS

#### 3.1 AERODYNAMIC WIND TUNNEL (1T)

The experiments were conducted in the Aerodynamic Wind Tunnel (1T), which is a continuous-flow transonic tunnel with atmospheric intake and exhaust. The test section is of square cross section, nominally 12 by 12 in. and 37.5 in. long, and is enclosed within a plenum chamber. Stagnation pressure is fixed at approximately 2,850 psfa with slight variations attributable to tunnel resistance and ambient pressure. To prevent water vapor condensation in the test section, stagnation temperature is normally varied within the range of 150 to 190°F as required.

Supersonic flows are established in the Mach number range of 1.1 to 1.5 with a two-dimensional flexible nozzle. Subsonic and transonic flows are obtained with a sonic nozzle contour in conjunction with adjustments in the tunnel backpressure and with plenum suction through an auxiliary evacuation system.

The tunnel test section configuration consisted of solid, planar sidewalls with several contoured, solid bottom walls to generate differing pressure distributions within the test region. The bottom wall (floor) was attached to the nozzle exit with a flexure, and the downstream end of the wall was supported by a remotely controllable jack-screw. Using the jack-screw, variations in wall angle,  $\theta_w$ , of  $\pm 1$  deg relative to the tunnel centerline were set (convergence is considered positive). The ventilated wall specimens were installed at the top (ceiling) of the test section, parallel to the tunnel centerline.

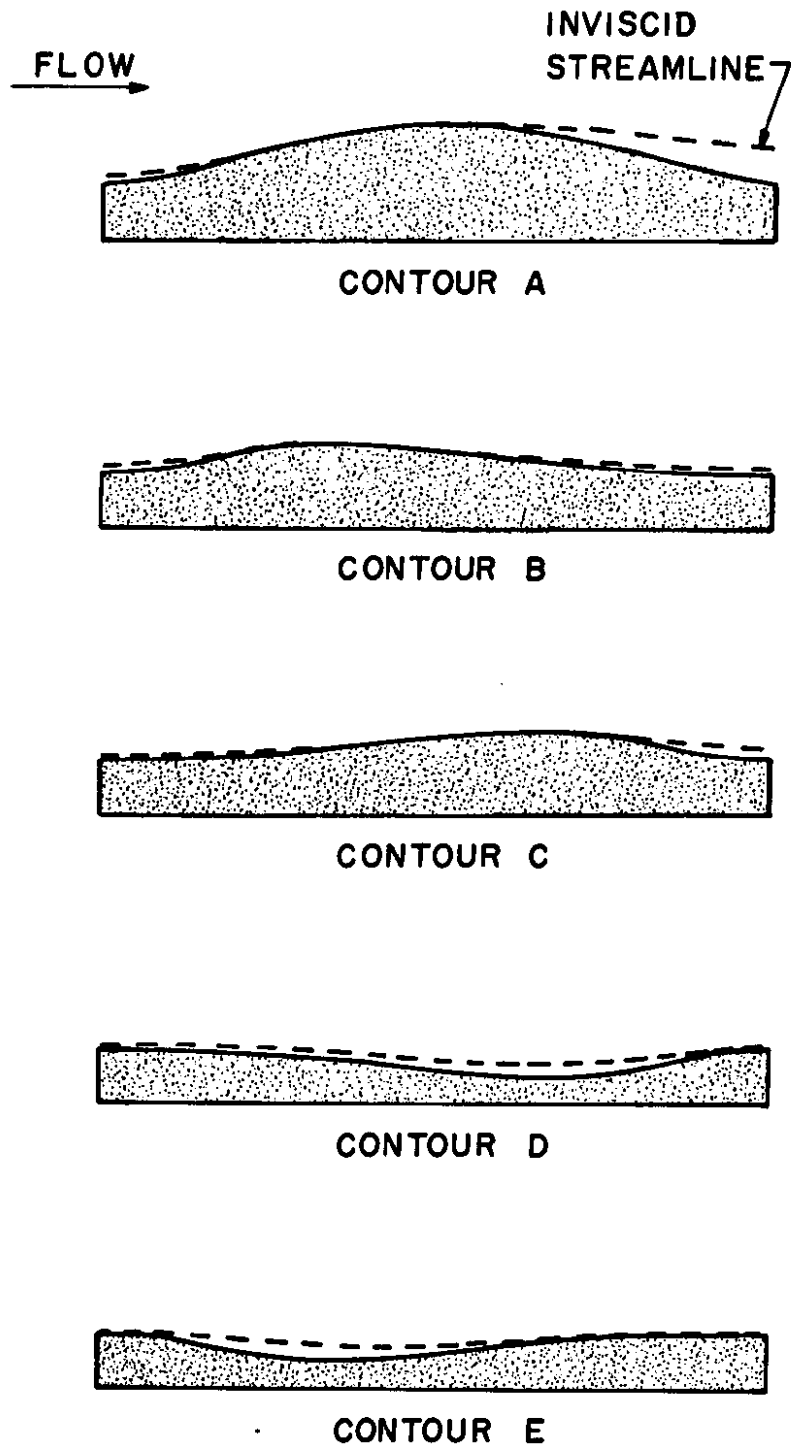
As applied to the tunnel geometry, the coordinate system of Fig. 1 is referenced to the nozzle exit, bottom wall, with the x-axis parallel to the tunnel centerline. All length dimensions where cited are in units of inches, with axial location usually phrased as tunnel station, that is, the distance downstream from the nozzle exit.

### 3.2 PRESSURE DISTURBANCE GENERATORS

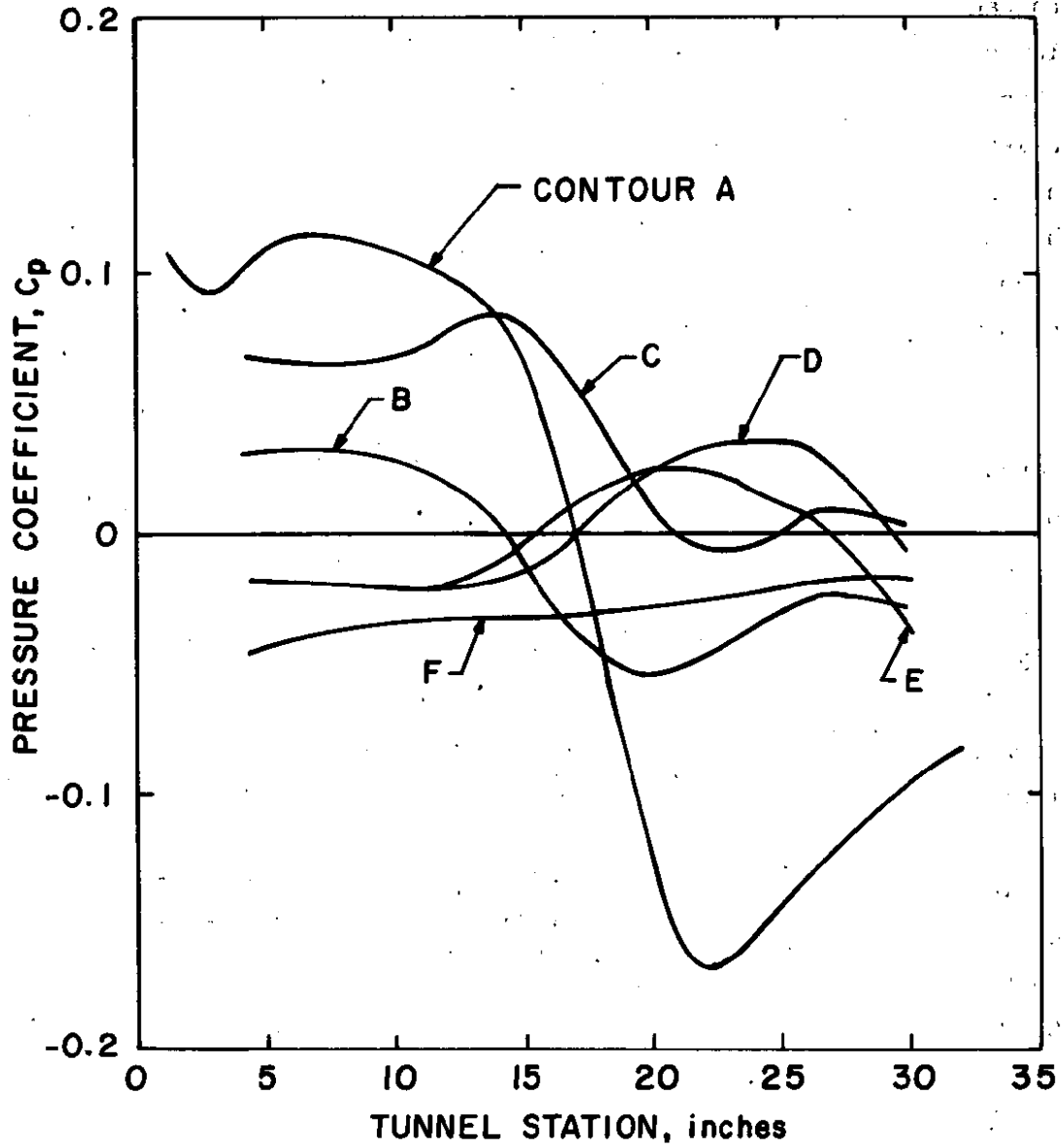
Lifting models in conventional ventilated wind tunnels generate far-field disturbances which, after interacting with the tunnel boundary as a whole, can be treated as simple pressure distributions imposed on the ventilated walls. To simulate the resulting pressure distributions in a manner amenable to analysis, several two-dimensional bottom-wall bumps were fabricated with rather arbitrary contours as disturbance generators. The profiles of the contours are presented in Fig. 5a. Each bump (nominally 12 in. in length) including a flat plate (Contour F) was installed with the leading edge at tunnel station 13. Upstream and downstream of the contours, flat-plate extensions were used. Unless indicated otherwise, data presented were obtained using the thickest bump (Contour A) with the bottom wall parallel to the tunnel centerline.

The dashed lines in Fig. 5a represent the boundary-layer displacement thickness development over the various contours. The calculations were based on the potential flow solution, with integration of the flow inclination at the bottom wall compatible with the measured pressures at  $M = 0.8$ . The resulting effective aerodynamic contours changed as functions of Mach number, wall angle, and ventilated wall geometry. Boundary-layer separation evidently occurred on all of the bottom wall contours (except the flat plate) so that the only viable method of solving for the interior potential flow field was the inverse technique.

An illustration of the types of pressure distributions achieved at the ventilated wall with the various disturbance generators is given in Fig. 5b. Again, it should be noted that variations in Mach number, bottom wall angle, or ventilated wall geometry significantly affected the resulting pressure distributions.



a. Geometric and effective contours  
Figure 5. Characteristics of the pressure disturbance generators.



b. Pressure distributions at the ventilated wall  
Figure 5. Concluded.

### 3.3 PERFORATED WALL GEOMETRY

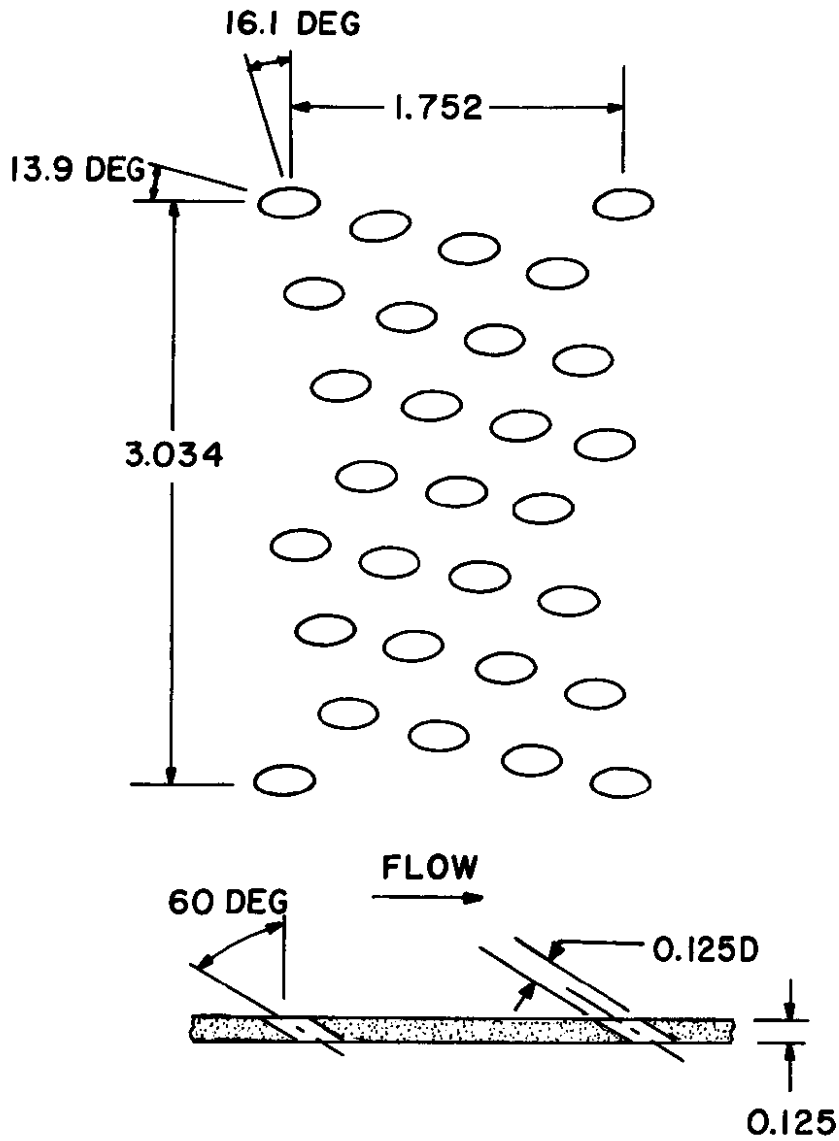
Four basic wall configurations were tested, denoted A through D, with each being based on the 60-deg inclined hole perforated wall developed at AEDC (Ref. 1). Pertinent dimensions of each wall are given in Fig. 6. Configuration D (Fig. 6c) was a variable-porosity wall consisting of two match-drilled plates with the airside plate held stationary and the backside or cutoff plate translated streamwise to achieve variations in porosity. For convenience, upstream movement of the cutoff plate for decreasing porosity is labeled positive porosity and downstream movement negative.

Perforated walls in transonic wind tunnels generate noise, termed edgetones, that is thought to degrade the quality of model test data. Two methods of suppressing the edgetones have been developed (and configurations A and D were tested with each). One modification consisted of inserting a splitter plate, SPL (Ref. 13) in each hole, longitudinally bisecting the hole, with the splitter-plate dimensions being 0.012 in. wide and 0.063 in. deep. The second modification consisted of a screen attached to the airside plate surface; in this instance the screen was of 40 by 60 mesh with 0.006 in. wire diameter.

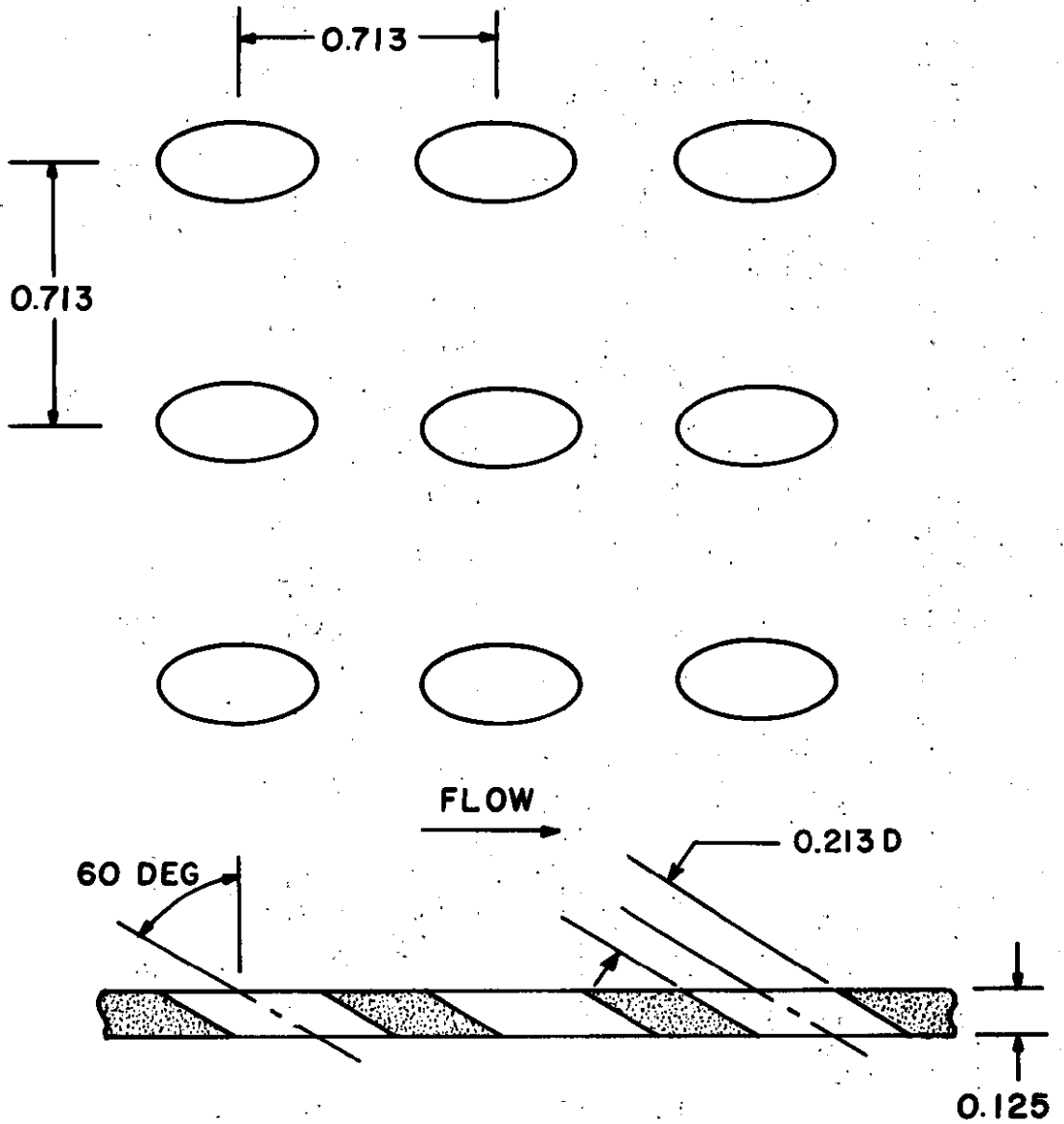
To distinguish among the differing wall geometries the configuration code is followed by wall porosity and, if appropriate, either SPL or SCR to denote the noise suppression device present (for example, D-1.0 SCR). Data are presented for 20 distinct ventilated wall geometries.

### 3.4 INSTRUMENTATION

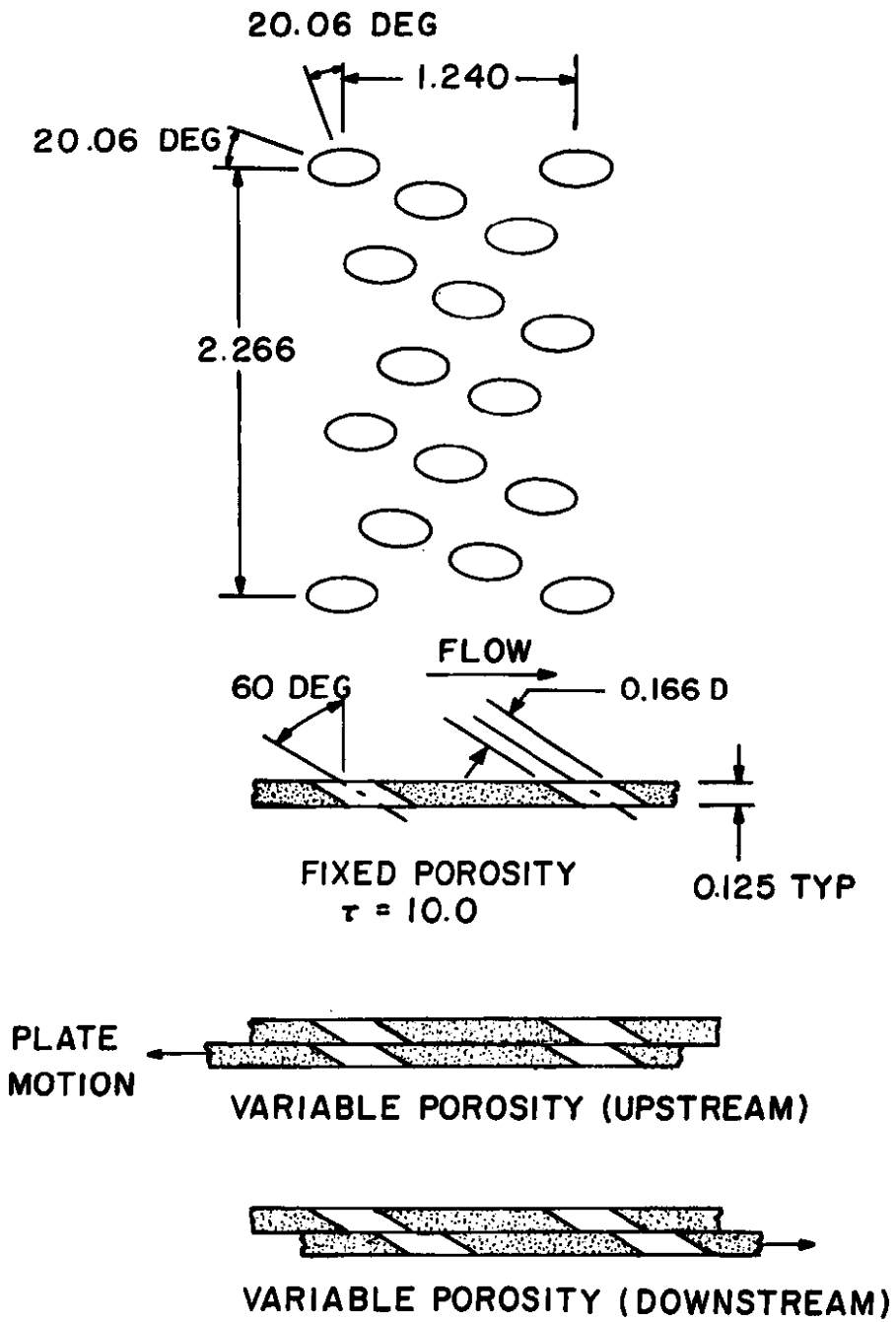
Primary tunnel parameters and the respective instrumentation used to sense and measure the parameters included: plenum pressure measured by a servo-driven precision mercury manometer; stagnation and diffuser exit pressures measured with strain-gage transducers referenced to the



a. Configuration A  
Figure 6. Perforated wall geometry.



b. Configuration B  
Figure 6. Continued.



c. Configuration C and D  
Figure 6. Concluded.

plenum pressure; and stagnation temperature measured with an iron-constantan thermocouple. Other pressure measurements were accomplished with five 48-port Scanivalves<sup>®</sup> using strain-gage transducers referenced to plenum pressure. These data were recorded with an on-line computer system. Raw data were recorded on punched paper tape, and results were tabulated in engineering units to aid in conducting the tests. The paper tape was subsequently processed to obtain the results presented herein.

Flow angularity measurements were obtained in the proximity of selected ventilated walls using laser velocimetry (LV) with a system described in Ref. 15. This system is a two-component, dual-scatter, moving fringe-type system operated in the off-axis, backscatter collection mode. On-line indication of the two velocity components was available from the data processor, but all results presented were processed off-line from digital magnetic tape recordings of the raw data.

Static pressure measurements in the vicinity of the ventilated walls were first made using a 0.5-in.-diam static pipe extending from the stagnation chamber through the nozzle and test section. With the pipe centerline nominally 1.25 in. below a perforated wall, it was discovered that the measured pressures were slightly dependent on the orientation of the orifice. The crossflow velocity component induced a variation in static pressure around the circumference of the pipe. Further complications, such as orifice-edge aberrations and nonrepairable leaks, forced abandonment of the static-pipe concept, although some data are presented. The test section sidewall was selected as the location for the all-important static pressure measurements near the ventilated walls. The measurements required for upstream and downstream boundary conditions were also made at the tunnel sidewall; however, pressure measurements for the bottom wall were obtained on the centerline.

A limited number of boundary-layer surveys was made with multiple-tube pitot pressure rakes. These data were reduced to the conventional parameters of displacement and momentum thicknesses assuming isoenergetic flow with Prandtl number equal to one.

## 4.0 PROCEDURE

### 4.1 TEST PROCEDURE

Tunnel test section conditions were unconventional in that there was, in general, no region of uniform flow. The disturbance field of the contoured bottom walls extended into the nozzle so that, at first glance, there is no free-stream Mach number for use in Eq. (1). However, the presence of one ventilated wall allows the introduction of a pseudo Mach number, the so-called plenum Mach number, which is simply a Mach number computed on the basis of an isentropic expansion from the stagnation pressure to the plenum pressure. It is emphasized that the flow within the plenum chamber actually was at a very low velocity. The pressure differences across ventilated walls are normally small; hence, the plenum Mach number is a good approximation to the nonexistent far-field or free-stream Mach number.

Test conditions were established by adjusting the plenum suction flow rate and the diffuser exit pressure in such a way that the desired Mach number was set while simultaneously maintaining reasonably uniform pressure gradients at the downstream end of the test section. Data were obtained for each configuration at Mach numbers between 0.5 and 0.85. Limited data were acquired between Mach numbers of 0.9 and 1.2.

For some ventilated walls, the bottom wall angle was adjusted to achieve changes in the mean boundary-layer thickness over the ventilated wall. Convergence of the bottom wall forced more flow into the plenum, thereby thinning the boundary layer. Divergence of the bottom wall yielded the opposite effect.

## 4.2 PRECISION OF MEASUREMENTS

Uncertainties in the pressure measurements have been estimated at the 95-percent confidence level considering the effects of the precision and repeatability of the instrumentation. For most of the pressure measurements, three or more individual data points were acquired in sequence and averaged to minimize the influence of low-frequency, small-amplitude oscillations in the tunnel flow. These effects were combined using the Taylor series method of error propagation. The resulting uncertainties in the basic parameters are:

Mach number, $M$	$\pm 0.005$
Pressure coefficient, $C_p$	$\pm 0.006$
Wall angle, $\theta_w$	$\pm 0.02$
Displacement thickness, $\delta_1$	$\pm 0.03$

The laser velocimetry data were derived from an average of approximately 1,000 samples/point, yielding negligible random error. Bias errors introduced within the system or from particle lag were of unknown magnitude.

## 5.0 RESULTS AND DISCUSSION

### 5.1 ASSESSMENT OF ACCURACY

Calculation of the flow angularity distribution rather than making direct measurements leads to results of unknown accuracy. A highly complicated relationship exists between the precision of pressure coefficient measurements and the precision of the calculated flow angles. Additional uncertainties arise from the assumptions of small perturbations and two-dimensional flow.

To obtain a qualitative appraisal of accuracy, independent measurements of the flow angles were made for selected ventilated walls 1 in. from the walls and compared with calculations made for the same conditions. These results are presented in Fig. 7 in the form of flow angle as a function of tunnel station for wall configurations A6.0, B7.0, and C10.0. Limited transverse surveys with the LV system indicated the flow in the vicinity of the perforated walls was two-dimensional with no perturbations from discrete holes detectable 1 in. from the wall.

The general agreement between the two independent estimates of flow angle is considered excellent. It is evident that the inverse technique yields results of good accuracy and is experimentally far less demanding than direct measurements. For the larger crossflow velocities (flow angle) the comparisons in Fig. 7 indicate possible contamination of the results by boundary-layer growth on the sidewalls since the LV data are generally of larger magnitude. Enforcement of continuity on a two-dimensional basis and matching of a streamline at the bottom wall resulted in artificially increased outflow and decreased inflow at the ventilated wall.

To obtain an indication of the boundary-layer program accuracy, two types of experiments were conducted. The first setup consisted of replacing the ventilated wall with a solid wall and performing all measurements and calculations as if there were mass flux through the wall. The resulting magnitude of the computed mass flux was approximately 10 percent of that obtained with ventilated walls of moderate porosity. Again, the sidewall boundary-layer growth is suspected as the major cause of this discrepancy. Since the extremes of wall mass flux decreased with decreasing wall porosity, it is evident that the relative accuracy of the results is dependent on wall porosity.

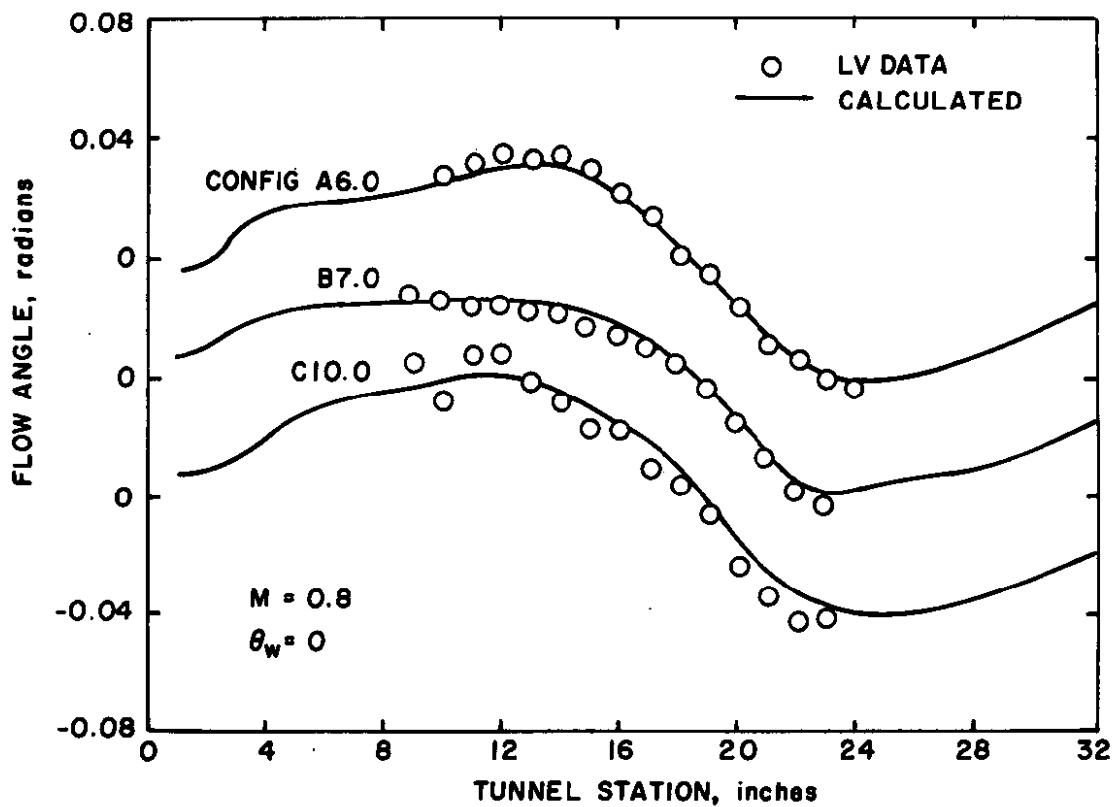


Figure 7. Comparison of calculated flow angle distributions with laser velocimetry measurement.

The second experiment consisted of measuring the boundary-layer profile at tunnel station 30 on configuration A6.0 with each of the bottom wall contours, with wall angle and Mach number as test variables. The resulting comparison of measured and calculated displacement thicknesses is presented in Fig. 8. The agreement of the two was considered excellent, and it was therefore assumed that the boundary-layer calculations were equally valid at other tunnel stations. Boundary-layer measurements were not made on any other ventilated wall geometry, which required the assumption that the effects of changes in wall geometry were fully reflected in the resulting distribution of flow inclination.

Since the calculated displacement thickness evidenced significant variation over the ventilated wall extent, the selected approach for analysis was to obtain the average thickness directly above the bottom wall contours.

## 5.2 PERFORATED WALL CHARACTERISTICS

### 5.2.1 Definition of the Wall Characteristic

As a means of introduction, a set of results obtained with configuration A6.0 is presented as a function of tunnel station in Fig. 9. Note that the static pressure distribution is the only experimental result with flow angle, wall mass flux, and boundary-layer displacement thickness being derived quantities. The measured pressure distribution was in general not sufficiently regular for the numerical computational procedure, and a moderate amount of data smoothing was employed. For a given fraction of irregularity in pressure coefficient, the resulting irregularity in flow angle was magnified with mass flux irregularities magnified again. This amplification of errors introduces fluctuations in the crossflow characteristic that have no physical meaning and should be ignored. As a consequence, the calculated wall mass flux was considered to be of insufficient accuracy to allow correlation of the wall characteristics and the flow angle was used for this purpose.

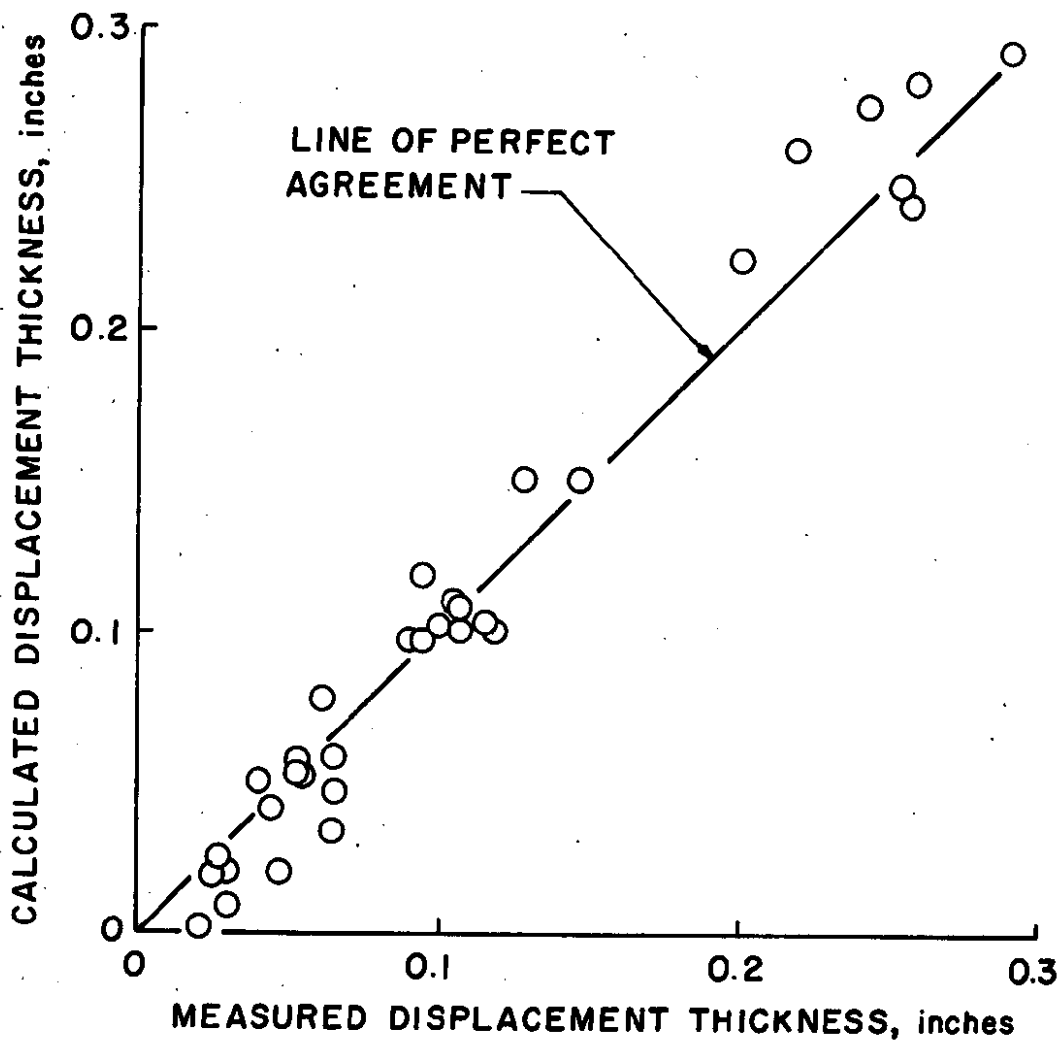


Figure 8. Comparison of calculated and measured boundary-layer displacement thickness.

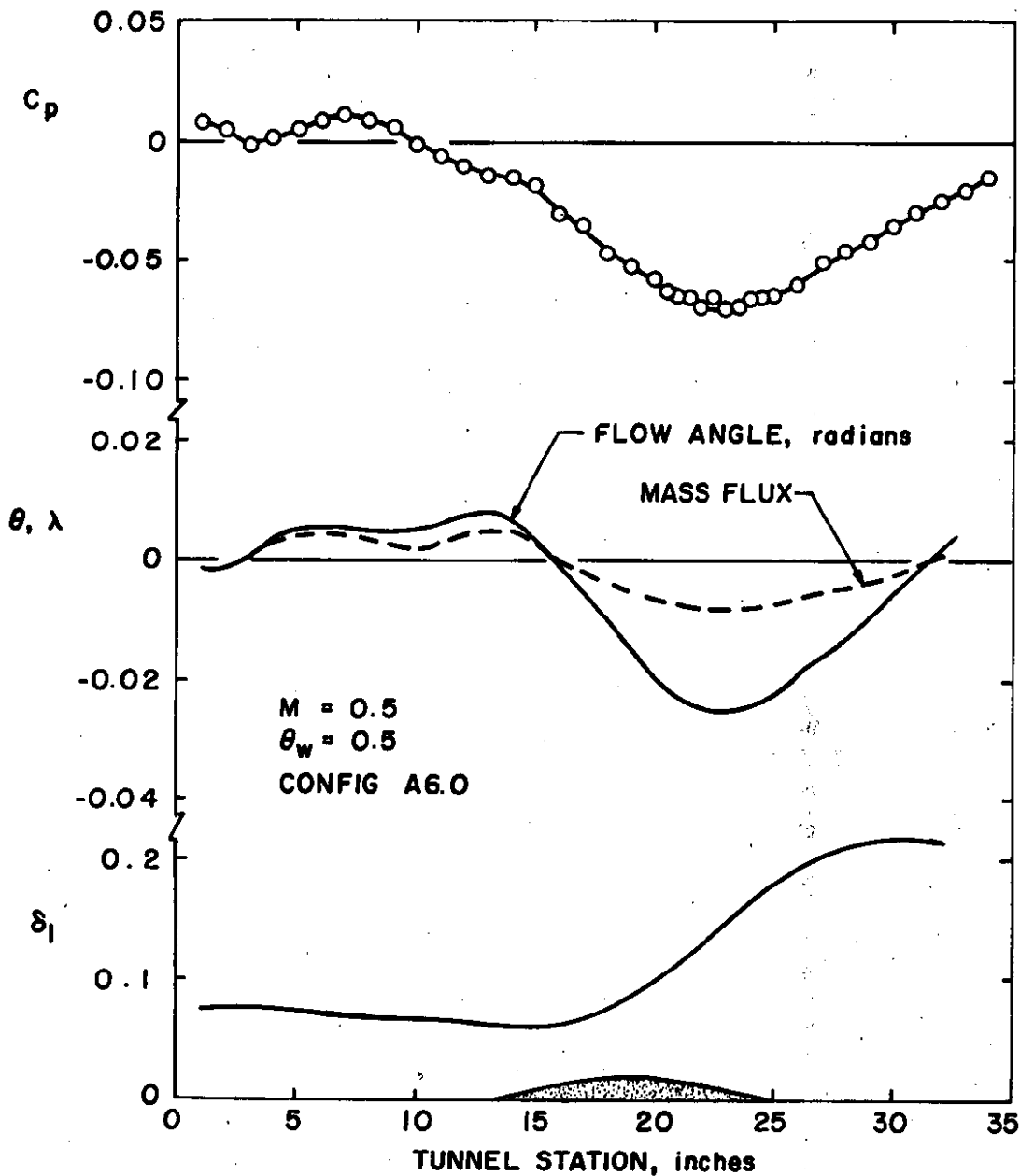


Figure 9. Representative variation of pressure coefficient, flow inclination, wall mass flux, and boundary-layer displacement thickness with tunnel station.

Techniques are available (Refs. 16 and 17) for wall interference correction of model test data, but little information is available concerning the proper boundary condition to represent the wind tunnel walls. The classical perforated boundary condition typically employed for subsonic wall interference calculations may be written as

$$\phi_x + \frac{\beta}{R} \phi_y = 0 \quad (11)$$

where  $\beta$  is the Prandtl-Glauert factor and  $R$  represents an unknown porosity factor or wall permeability. Equation (11) is a linearized approximation to viscous flow through a porous medium where the average velocity normal to the wall is assumed proportional to the pressure drop through the wall, and the pressure outside the wall is assumed equal to the free-stream pressure. In terms of experimental data for perforated wall characteristics, the locus of pressure coefficient and flow angle provides the required boundary condition in the form of

$$\frac{\beta}{R} = \frac{1}{2} \frac{dC_p}{d\theta} \quad (12)$$

Thus, for utilization of the present results within existing theoretical wall interference prediction methods, there should exist a linear relationship between  $C_p$  and  $\theta$ . A representative crossplot of pressure coefficient as a function of flow angle is presented in Fig. 10 wherein the streamwise path is denoted by directional arrows and the leading- (LE) and trailing-edge (TE) tunnel stations of the bottom wall contour were as indicated. The characteristics were obviously not linear at the upstream portion of the wall, although reasonable linearity existed over and downstream of the bottom wall contour. The upstream portion of the perforated wall was used to establish flow conditions, whereas normally four ventilated walls would be utilized at significantly less model blockage ratios; therefore, it is suggested that the data obtained directly above the contour were more representative of conventional conditions.

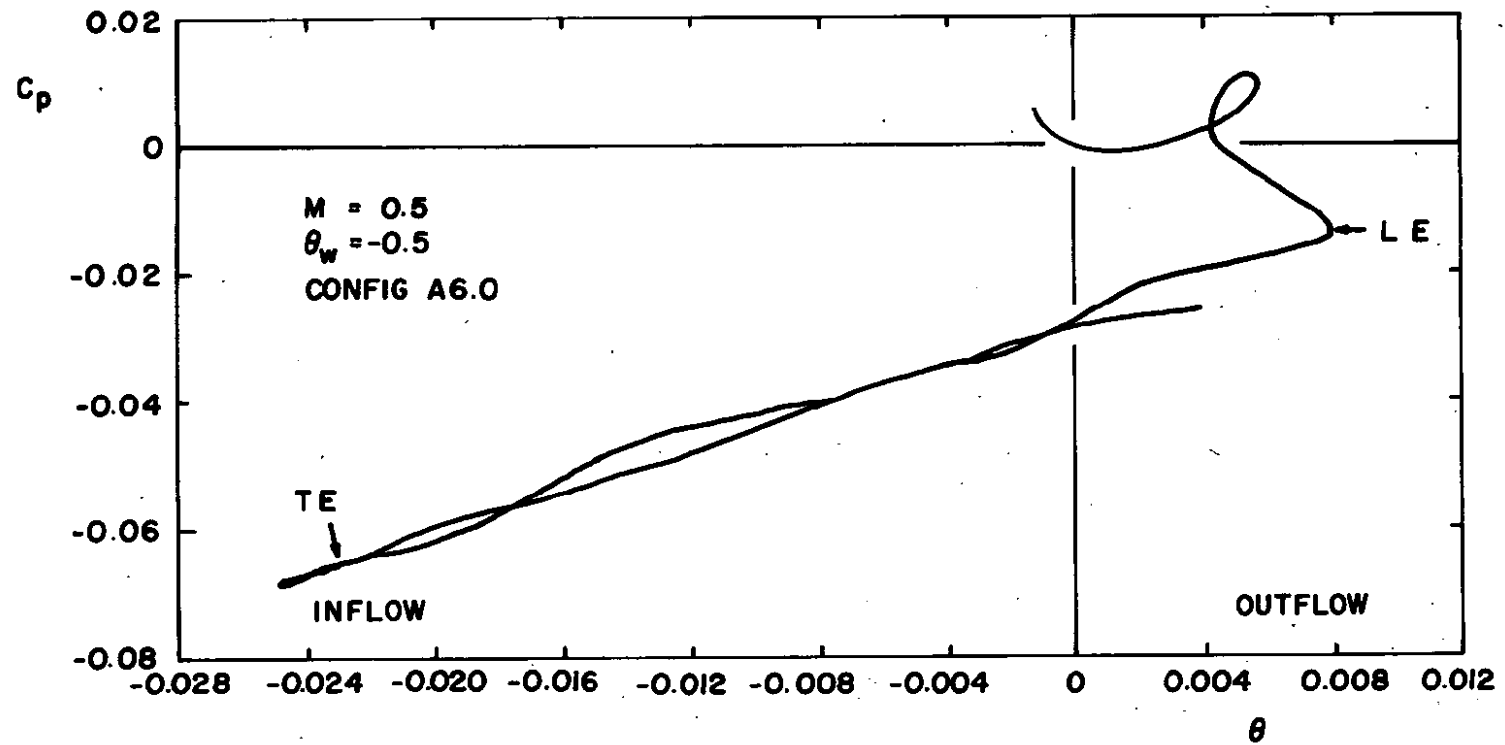


Figure 10. Representative locus of pressure coefficient and flow inclination - the wall characteristic.

To quantify the wall characteristics, a least-squares, linear fit of the  $C_p - \theta$  locus was obtained; this fitting was limited to the wall region directly above the bottom wall contour. The resulting slope and intercept were taken to be the primary descriptors of the ventilated wall characteristics.

Representative  $C_p - \theta$  loci for each wall configuration are given in Appendix A. The origin of each curve is displaced for clarity. Again, it should be noted that these data were obtained with the bottom wall parallel to the tunnel centerline with the circular arc (Contour A) installed.

### 5.2.2 Influence of Boundary-Layer Thickness on the Characteristic Slope

The effect of changes in the imposed pressure distribution as achieved with the differing bottom wall contours and wall angle is presented in Fig. 11. These results were obtained with configuration A6.0 at  $M = 0.6$ . It is clear that a unique wall characteristic does not exist in the sense of previous investigations. The shape of the  $C_p - \theta$  locus is dependent on the pressure distribution. Furthermore, the mean slope decreases as the boundary layer is thickened because of either bottom wall divergence or reduced contour height.

A quantitative description of the wall characteristic dependence on the boundary-layer displacement thickness is presented in Fig. 12. These data were obtained with variations of the bottom wall geometry. If the characteristic is reasonably linear (see Appendix A), then the slope is correlated by the ratio of the average displacement thickness to the hole diameter with the exception of a few (inexplicable) outlying points, the correlation indicating decreased slope with increased thickness. This approach was consistent in that both the characteristic slope and the boundary-layer thickness were averages over the wall extent directly above the bottom wall contours.

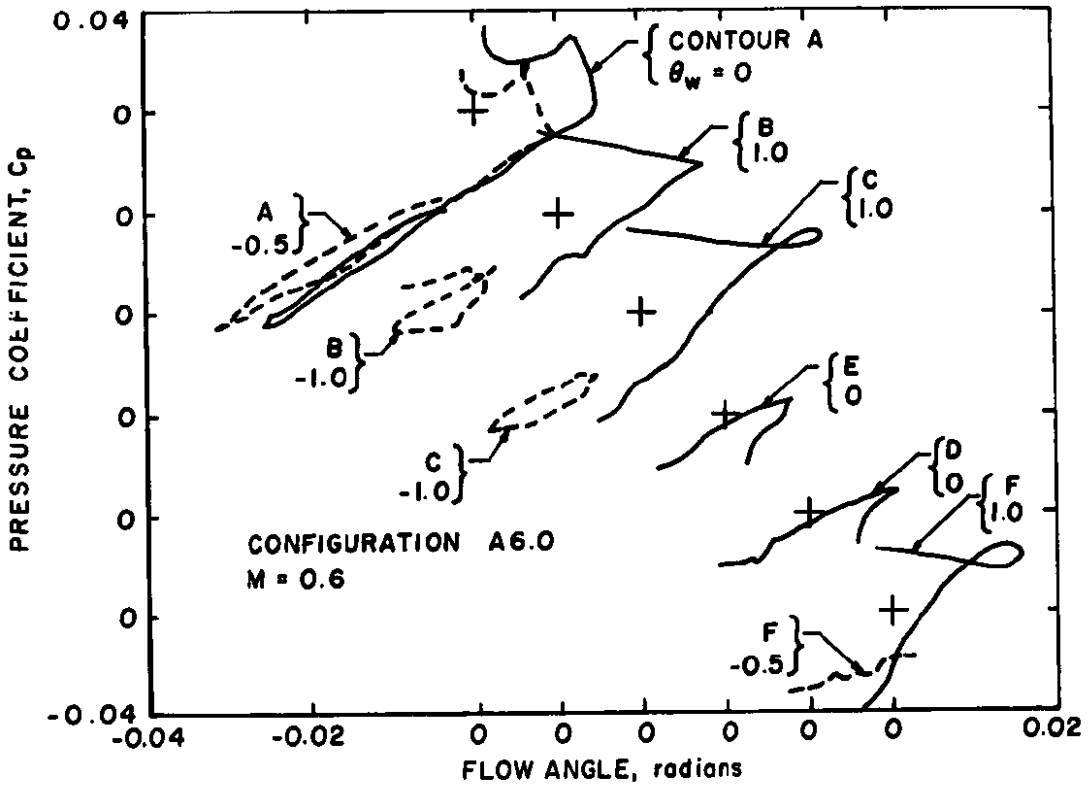
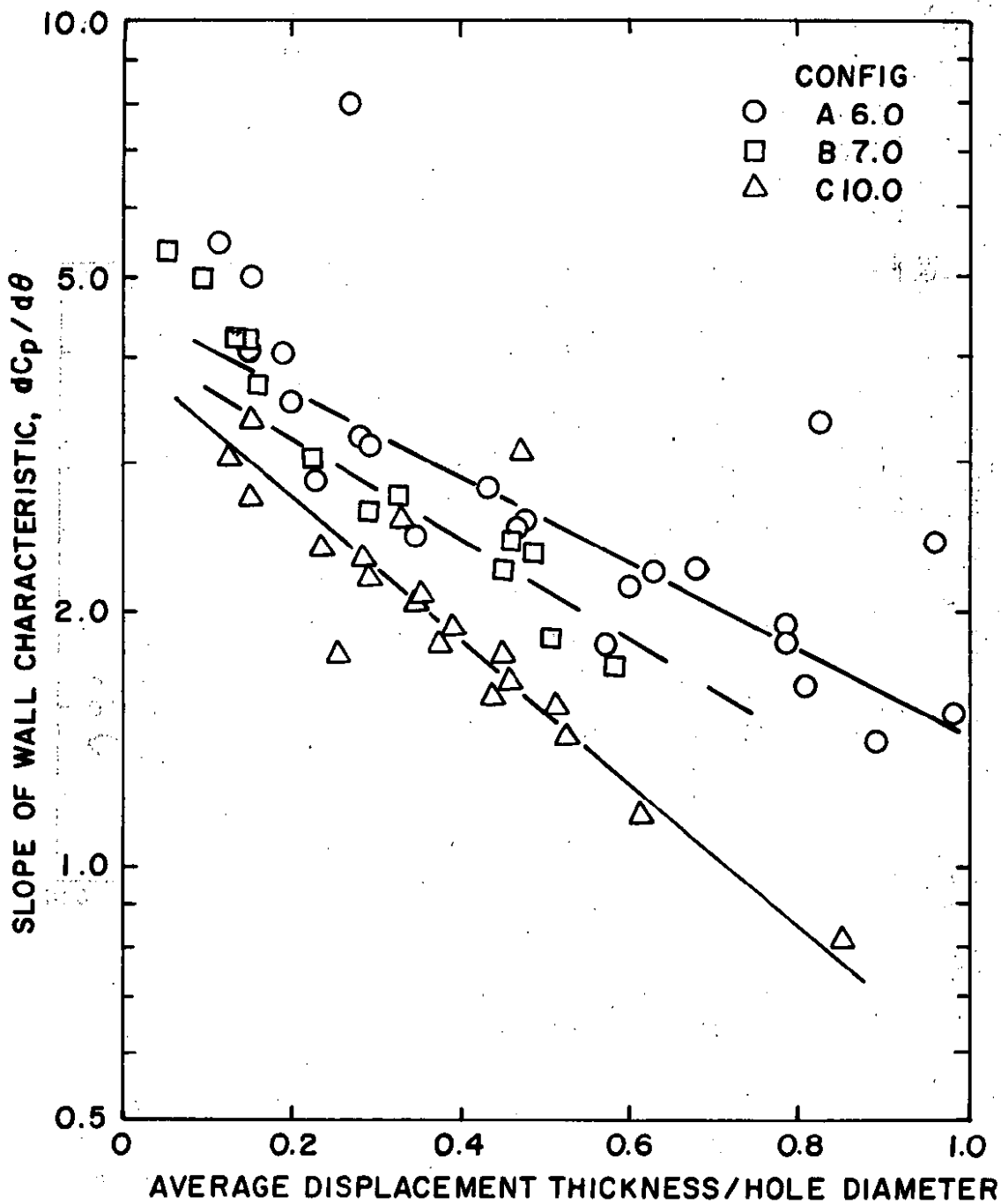
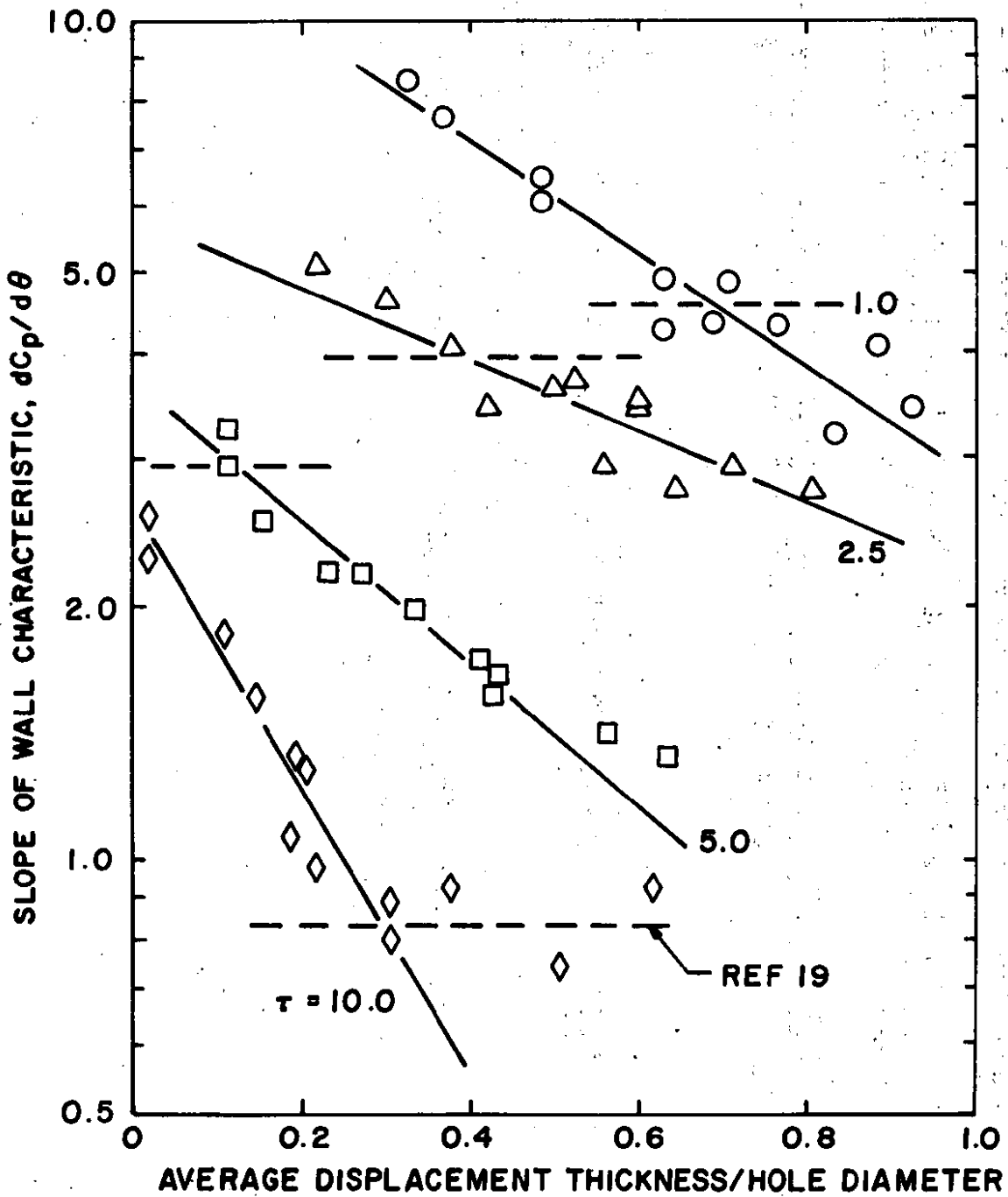


Figure 11. Variability of the wall characteristic with changes in the imposed pressure distribution.



a. Fixed porosity walls

Figure 12. Effect of boundary-layer displacement thickness on the characteristic slope.



b. Configuration D  
Figure 12. Concluded.

It is evident that the slope of the wall characteristic, and hence the boundary condition for wall interference estimates, is dependent on the relative thickness of the wall boundary layer. Anything that changes the boundary-layer thickness will change the wall characteristic. Since the tunnel wall boundary layer generally becomes thinner with increasing Reynolds number or with increased model size, the representative wall interference boundary condition is variable. Furthermore, a lifting model in a ventilated wind tunnel would generate disturbances at the wall such that, in general, the ceiling boundary layer would be thicker than that on the floor with resulting disparity in floor/ceiling boundary conditions. This conclusion is consistent with the findings of Mokry, et al. (Ref. 18) who attributed the difference in wall boundary conditions to a nonlinear wall characteristic. Reference 18 also demonstrated that increased Mach number increased the wall characteristic slope. This trend may now be interpreted to be the result of decreased boundary-layer thickness caused by an enlargement of the model disturbance field and additional suction at the wall.

The characteristics of configuration D with upstream movement of the cutoff plate are summarized in Fig. 12b. The variable porosity feature provides good control over the wall boundary condition. Also indicated in Fig. 12b are the results from a previous attempt (Ref. 19) at quantifying the characteristics of this wall geometry. Reasonable agreement is evident (same order of magnitude) except at five-percent porosity where no explanation of this discrepancy is apparent.

### 5.2.3 Influence of the Boundary-Layer Thickness on the Tunnel Calibration

The intercept of the  $C_p - \theta$  locus approximation was considered to be the best available estimate of the pressure drop across the walls corresponding to uniform flow conditions within a test section. These values are found to be correlatable with the average boundary-layer displacement thicknesses as presented in Fig. 13. These data indicate

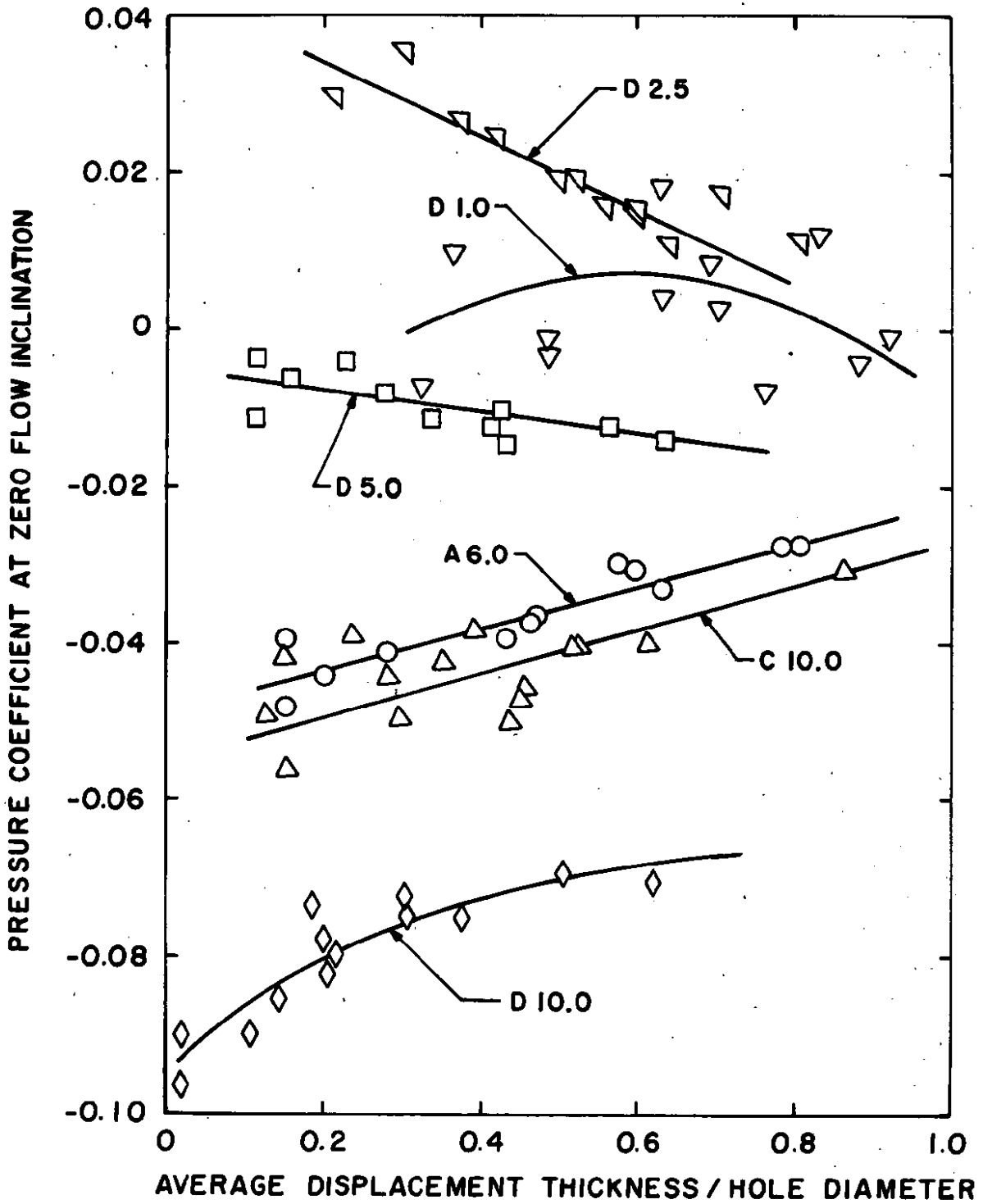


Figure 13. Effect of boundary-layer displacement thickness on the characteristic intercept.

significant variation of the wall pressure differential with changes in boundary-layer displacement thickness, which in turn affects the Mach number precision of conventional transonic wind tunnels. Current techniques of wind tunnel practice include calibration of the tunnel center-line Mach number against the plenum Mach number and subsequent use of that calibration to infer a free-stream Mach number from the plenum Mach number, regardless of the model blockage. Since the model installation tends to reduce the wall boundary-layer thickness relative to that occurring in the empty tunnel, the calibration becomes inapplicable. Admittedly, the error in Mach number would be small, but nonetheless present. A further source of imprecision in Mach number results from calibration at one Reynolds number and thence applying that calibration for tests at all available Reynolds numbers.

The sensitivity of test section Mach number to wall boundary-layer thickness suggests that the present practice of using plenum pressure to define a free-stream Mach number should be re-examined.

#### 5.2.4 Variable-Porosity Wall Geometry

As discussed in Section 3.3, the variable-porosity wall (configuration D) was tested with both upstream and downstream displacement of the cutoff plate. Examination of the  $C_p$ - $\theta$  loci in Fig. A-4 (Appendix A) clearly indicates distinct differences in the wall characteristics as a result of the cutoff plate movement direction. This difference is illustrated in more detail in Fig. 14, along with the theoretically required wall characteristics for alleviation of subsonic wall interference or supersonic wave reflection. The subsonic interference-free curve was calculated with the computer code described in Section 2.1, and the supersonic line is the result of small disturbance theory (Ref. 19). Configuration D with upstream cutoff plate movement reasonably matches the linear characteristic required for supersonic wave cancellation, and the downstream movement characteristic approximates the

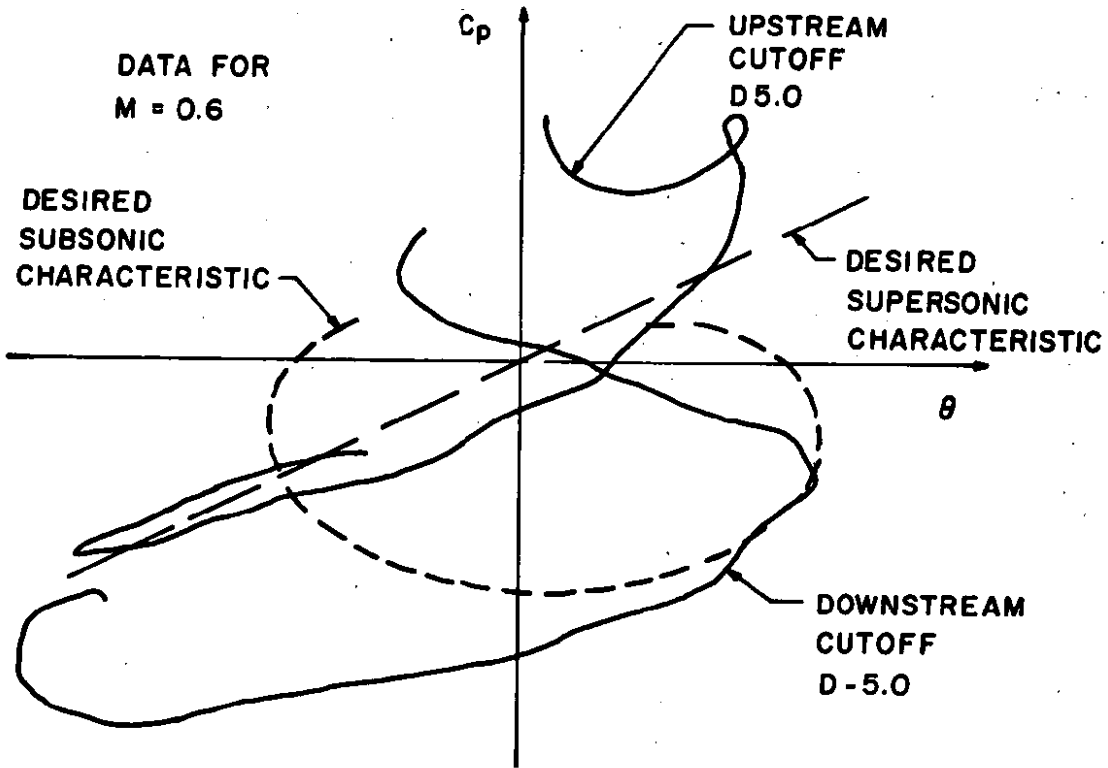


Figure 14. Comparison of the variable-porosity wall characteristics for upstream and downstream displacement of the cut-off plate.

cardioid-shaped  $C_p - \theta$  locus desired for subsonic flow (note the  $C_p$  origin is shifted to compensate for the different plenum Mach numbers).

Therefore, consideration should be given to using this variable-porosity wall with both upstream and downstream displacement of the cutoff plate as a function of Mach number.

### 5.3 EFFECT OF NOISE SUPPRESSION DEVICES

Several techniques (Refs. 13 and 14) have been developed for suppression of the edgetones, but it was not known what effect these wall modifications had upon the crossflow characteristic. As discussed in Section 3.3, two types of noise suppression devices were investigated: splitter plates (SPL) bisecting each hole and a screen overlay (SCR) on the airside surface. The crossflow characteristics obtained are presented in Appendix A.

For purposes of discussion, some data for wall configuration A are reproduced as Fig. 15. The changes in the characteristic resulting from the splitter-plate modification were an increased pressure drop across the wall and an enlarged spread of double-valuedness in  $C_p$  for fixed  $\theta$ . The multiple-value pressure for a given flow inclination, particularly inflow, is indicative of sensitivity to boundary-layer thickness and is thought to be evidence that the wave cancellation properties of the wall would be adversely affected. The change in pressure drop across the wall at zero crossflow velocity would change a tunnel calibration but have no other significant effect.

Results obtained with the screen overlay evidence an opposite trend in the inflow region of the wall characteristic relative to the splitter plate. The multiple-valued area was enlarged but resulted in a negative pressure shift with increased boundary-layer thickness. The effect of this change on the wave cancellation properties of the wall is unknown. The screen solidity was 30 percent, and one would intuitively expect

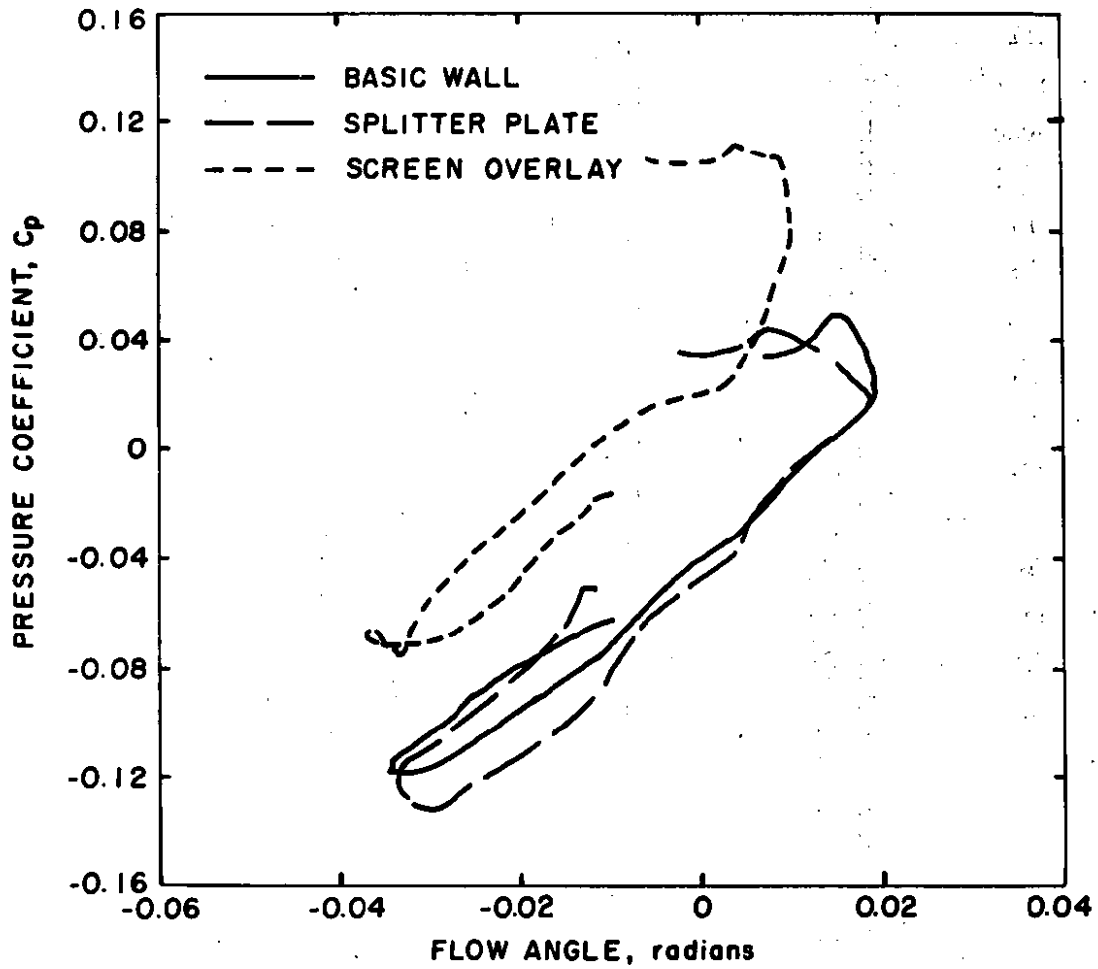
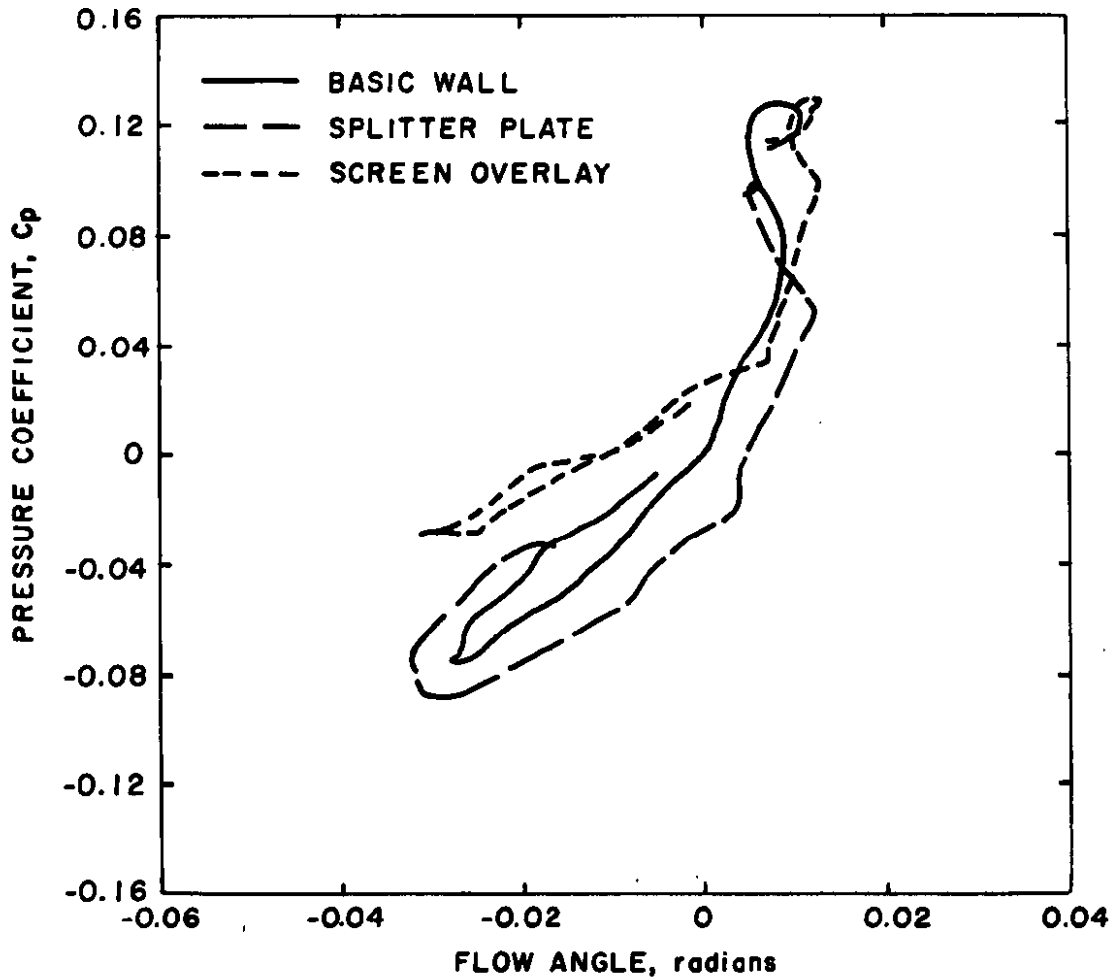


Figure 15. Effect of noise suppression devices on the characteristics of configuration A.

that the wall characteristic slope should have increased accordingly, but the least-squares slope was increased only 10 percent or less relative to that of the basic wall.

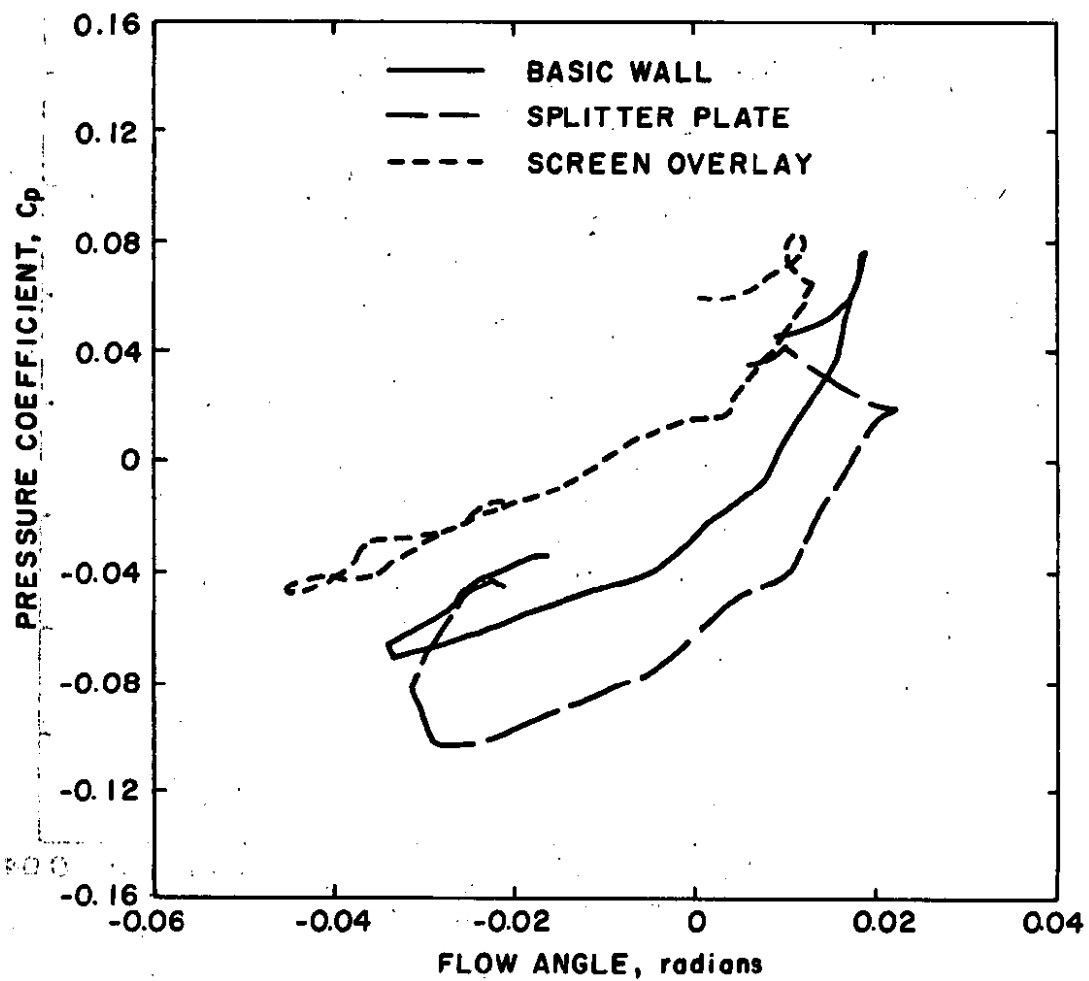
The effect of the noise suppression devices on the characteristics of wall configuration D are presented in Fig. 16 for selected porosities. Again, the splitter plate tended to open up the characteristic, which is believed to adversely affect the wave cancellation properties of the wall. On the other hand, the screen overlay tended to close the characteristic and yielded practically single-valued curves. These results indicate that a screen overlay on the variable-porosity wall would improve the supersonic wave cancellation properties. However, referring to Fig. 16, the screen overlay also straightened the characteristic with downstream movement of the cutoff plate which would remove any chance of achieving a reduced subsonic wall interference test environment.

In most instances, the screen overlay on configuration D tended to reduce the characteristic slope. The slope change does not affect the utility of the wall because the variable-porosity feature retains control of the wall characteristic.

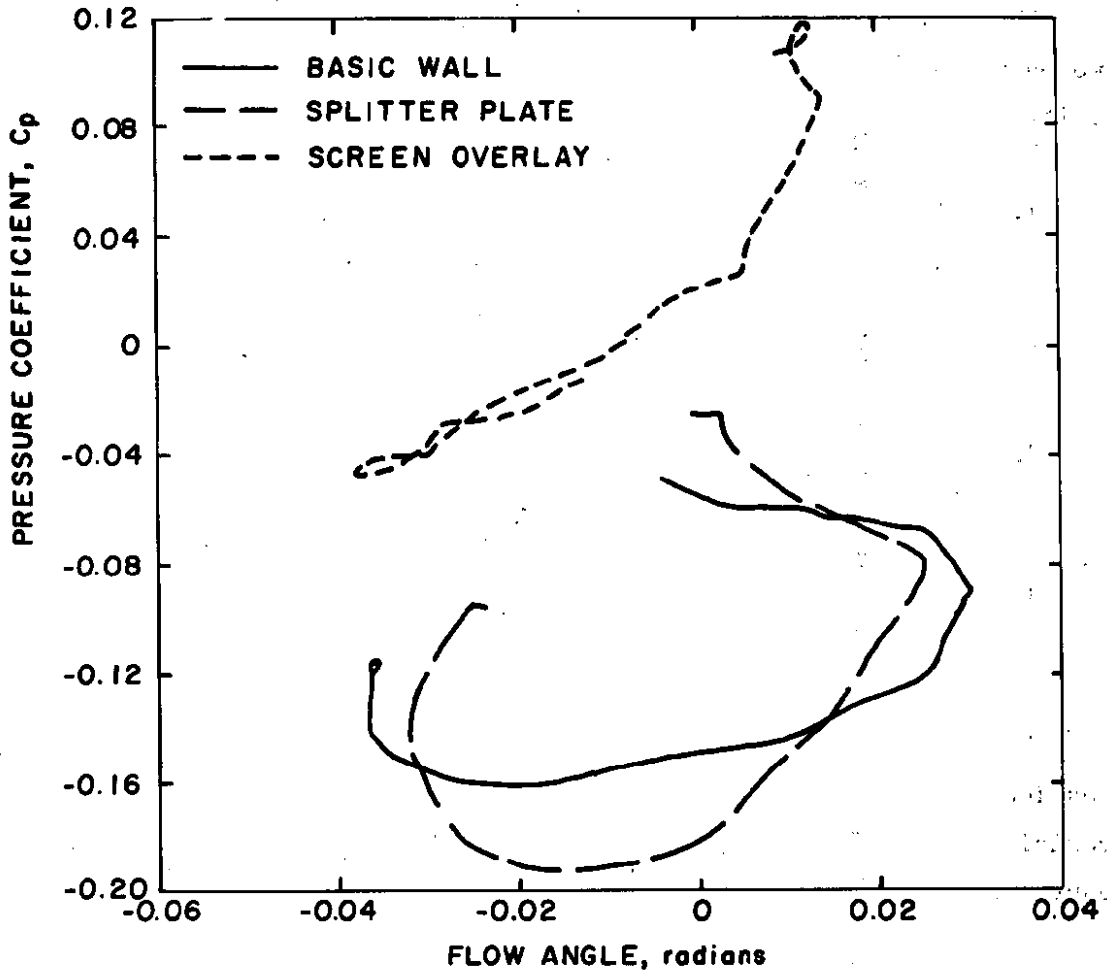


a.  $r = 2.5$  (upstream)

Figure 16. Effect of noise suppression devices on the characteristics of configuration D.



b.  $\tau = 5.0$  (upstream)  
Figure 16. Continued.



c.  $\tau = -5.0$  (downstream)  
Figure 16. Concluded.

## 6.0 CONCLUDING REMARKS

A method has been developed that allows sufficiently accurate determination of the crossflow characteristics of ventilated walls. The procedure enables direct comparison of the characteristics of different walls and requires the experimental measurement of static pressure only, the flow inclination being calculated from those measurements. The static pressure and flow inclination streamwise distribution in the vicinity of the wall then enables calculation of the boundary-layer development on, and mass flux through, the ventilated wall.

These techniques were employed to document the characteristics of two basic perforated wall geometries, fixed porosity and variable porosity with 60-deg inclined holes, with the following results:

1. The perforated wall crossflow characteristic, defined as the locus of pressure coefficient ( $C_p$ ) against flow angle ( $\theta$ ), is not unique and shows dependence on the longitudinal pressure distribution.
2. Increased boundary-layer thickness or increased porosity decrease the slope,  $dC_p/d\theta$ , of the wall characteristic.
3. The pressure drop across the wall at zero crossflow velocity is dependent on boundary-layer thickness.

The effects on the wall characteristic of two types of noise suppression devices, splitter plates bisecting each hole and a screen overlaid on the airside surface, were documented with the following results being obtained:

1. The splitter plates increase the pressure drop across the walls and open up (decreased single-valuedness) the wall characteristic.
2. The screen overlay decreases the pressure drop across the walls and tends to yield more linear characteristics.

Analysis of these results and their relationship with current wind tunnel operating procedures and practice has indicated the following conclusions:

1. The crossflow characteristic of most (not all) perforated walls can be assumed linear for purposes of calculating subsonic wall interference effects. However, each wall of the wind tunnel test section may require a different characteristic representation to accommodate differences in mean wall boundary-layer thicknesses.
2. If plenum pressure is sensed to indicate the free-stream Mach number via empty-tunnel calibration, the resulting test section Mach number will probably vary as a function of Reynolds number, model blockage, and possibly model attitude.

#### REFERENCES

1. Goethert, B. H. Transonic Wind Tunnel Testing. Pergamon Press, New York, 1961.
2. Chew, W. L., Jr. "Experimental and Theoretical Studies on Three-Dimensional Wave Reflection in Transonic Test Sections, Part III: Characteristics of Perforated Test-Section Walls with Differential Resistance to CrossFlow." AEDC-TN-55-44 (AD84158), March 1956.
3. Chew, W. L., Jr. "Characteristics of Perforated Plates with Conventional and Differential Resistance to Cross-Flow and Airflow Parallel to the Plates." Proceedings of the Propulsion Wind Tunnel Transonic Seminar, AEDC, July 1956.
4. Vidal, R. J., Erickson, J. C., Jr., and Catlin, P. A. "Experiments with a Self-Correcting Wind Tunnel." Advisory Group for Aerospace Research and Development AGARD CP-174, October 1975.

5. Berndt, S. B. and Sorensen, H. "Flow Properties of Slotted Walls for Transonic Test Sections." Advisory Group for Aerospace Research and Development AGARD CP-174, October 1975.
6. Murman, E. M. and Cole, J. D. "Calculation of Plane Steady Transonic Flows." AIAA Journal, Vol. 9, No. 1, January 1971.
7. Liepmann, H. W. and Roshko, A. Elements of Gasdynamics. John Wiley and Sons, New York, 1958.
8. Murman, E. M. "Analysis of Embedded Shock Waves Calculated by Relaxation Methods." Proceedings of the AIAA Computational Fluid Dynamics Conference, Palm Springs, California, July 1973.
9. Milne-Thomson, L. M. Theoretical Hydrodynamics. The Macmillan Company, 1968.
10. Lukasiewicz, J. "Effects of Boundary Layer and Geometry on Characteristics of Perforated Walls for Transonic Wind Tunnels." Aerospace Engineering, April 1961.
11. Whitfield, D. L. "Analytical, Numerical, and Experimental Results on Turbulent Boundary Layers." AEDC-TR-76-62 (AD-A027588), July 1976.
12. Patankar, S. V. and Spalding, D. B. Heat and Mass Transfer in Boundary Layers. Morgan-Grampian, London, 1967.
13. Dougherty, N. S., Jr., Anderson, C. F., and Parker, R. L., Jr. "An Experimental Investigation of Techniques to Suppress Edgetones from Perforated Wind Tunnel Walls." AEDC-TR-75-88 (AD-A013728), August 1975.

14. Schutzenhofer, L. A. and Howard, P. W. "Suppression of Background Noise in a Transonic Wind-Tunnel Test Section." AIAA Journal, Vol. 13, No. 11, November 1975.
15. Cline, V. A. and Lo, C. F. "Application of the Dual-Scatter Laser Velocimeter in Transonic Flow Research." Proceedings of the AGARD Symposium on Application of Non-Intrusive Instrumentation in Fluid Flow Research, France, May 1976.
16. Garner, H. C., Rogers, E. W. E., Acum, W. E. A., and Maskell, E. C. "Subsonic Wind Tunnel Wall Corrections." Advisory Group for Aerospace Research and Development, AGARDograph 109, October 1966.
17. Pindzola, M. and Lo, C. F. "Boundary Interference at Subsonic Speeds in Wind Tunnels with Ventilated Walls." AEDC-TR-69-47 (AD687440), May 1969.
18. Mokry, M., Peake, D. J., and Bowker, A. J. "Wall Interference on Two-Dimensional Supercritical Airfoils, Using Wall Pressure Measurements to Determine the Porosity Factors for Tunnel Floor and Ceiling." National Research Council NRC No. 13894, February 1974.
19. Jacocks, J. L. "Evaluation of Interference Effects on a Lifting Model in the AEDC-PWT 4-Ft Transonic Tunnel." AEDC-TR-70-72 (AD868290), April 1970.

APPENDIX A  
COMPARATIVE CROSSFLOW CHARACTERISTIC DATA  
FOR EACH PERFORATED WALL GEOMETRY

Comparison of the characteristics of one ventilated wall geometry with another geometry is fully realistic only if all other variables are fixed, specifically the imposed pressure distribution and wall boundary-layer thickness. Since this situation could not be achieved, an alternate presentation of the results is given herein with fixed pressure disturbance geometry. The characteristics of each perforated wall were measured with the circular arc contour installed with the bottom wall parallel to the tunnel centerline. These data are presented for Mach numbers of 0.5, 0.6, 0.7, and 0.8 with offset origins in Figs. A-1 through A-8. Comparisons among the data are meaningful in the sense of wall performance in a conventional wind tunnel with fixed model geometry.

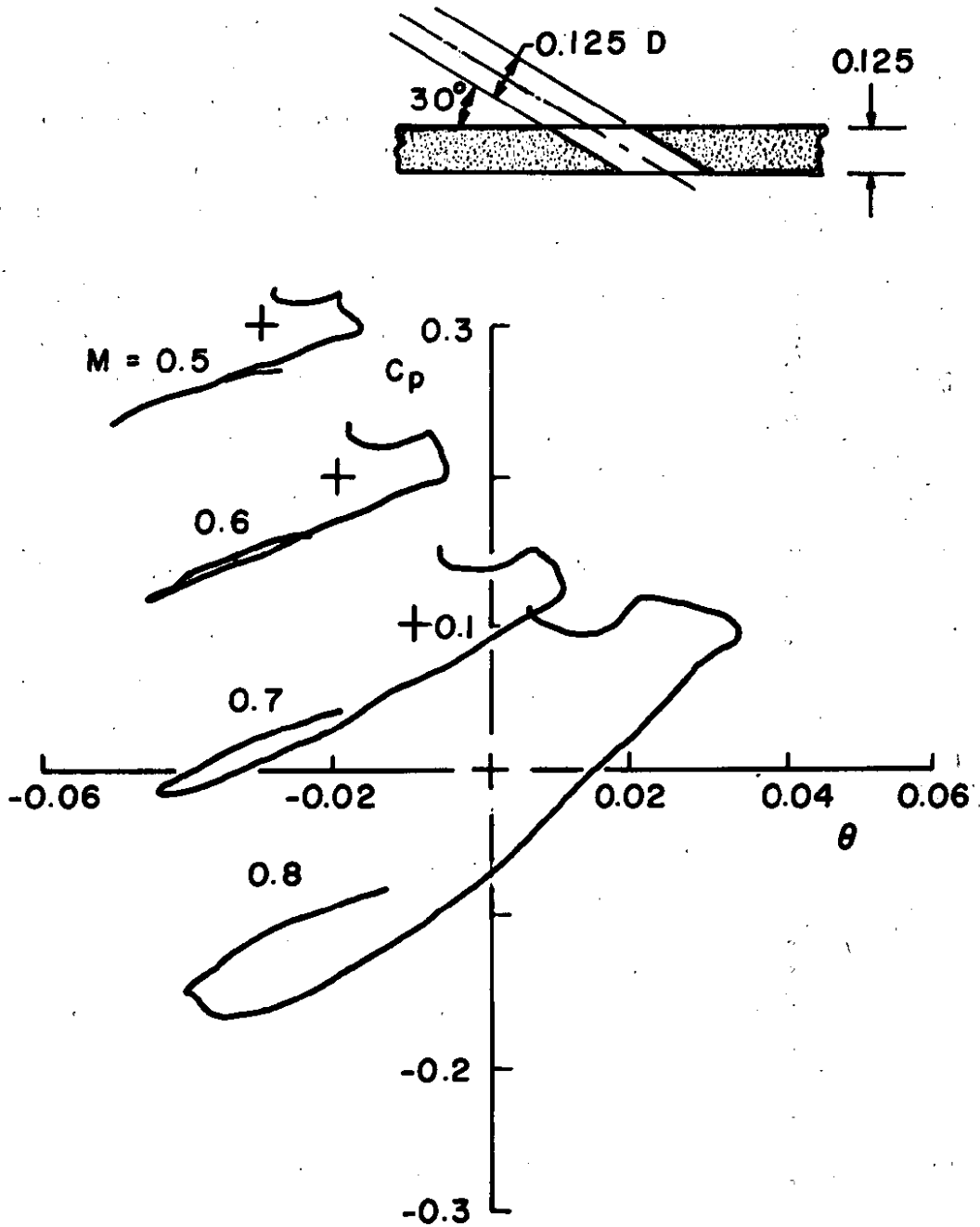


Figure A-1. Characteristics of configuration A6.0.

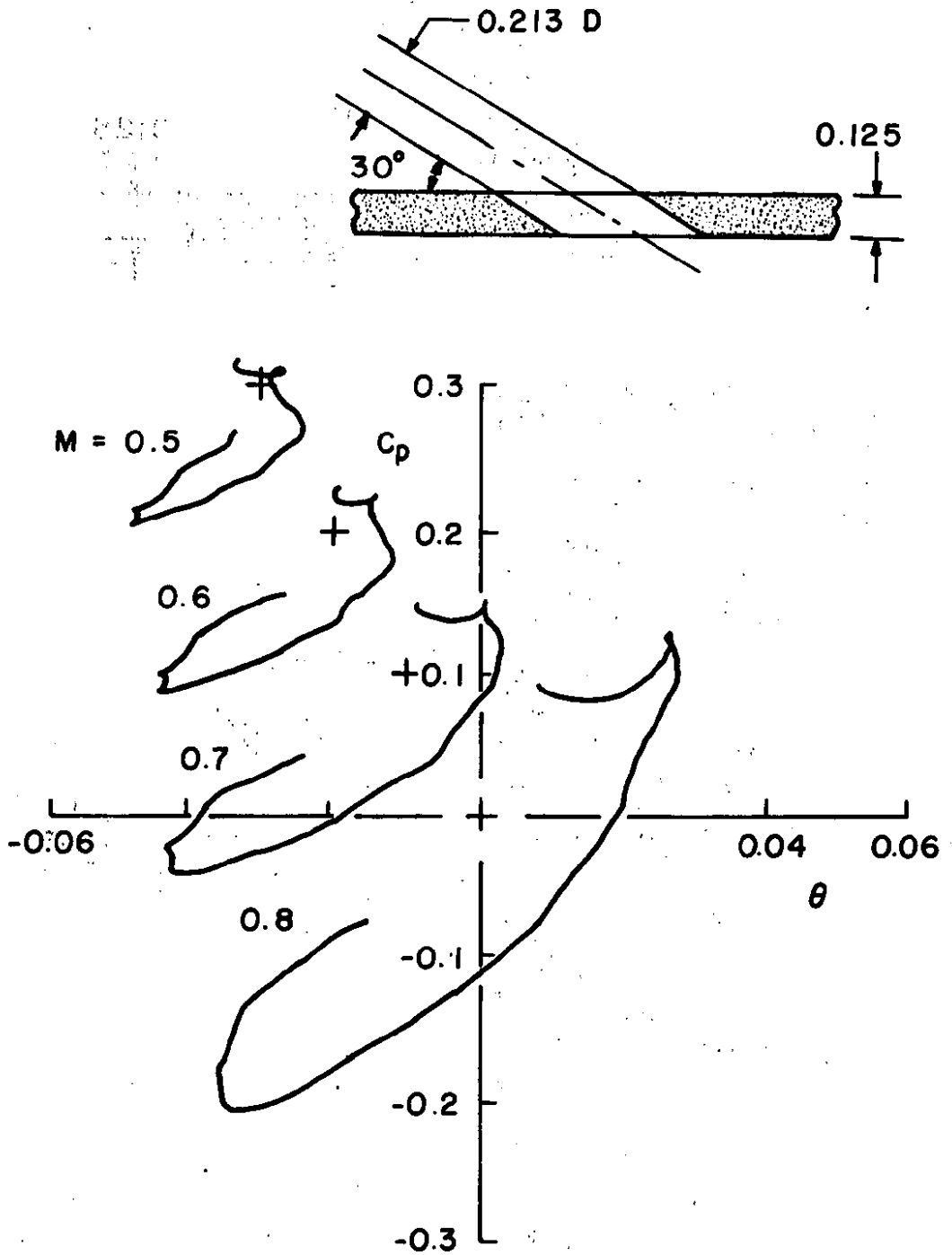


Figure A-2. Characteristics of configuration B7.0.

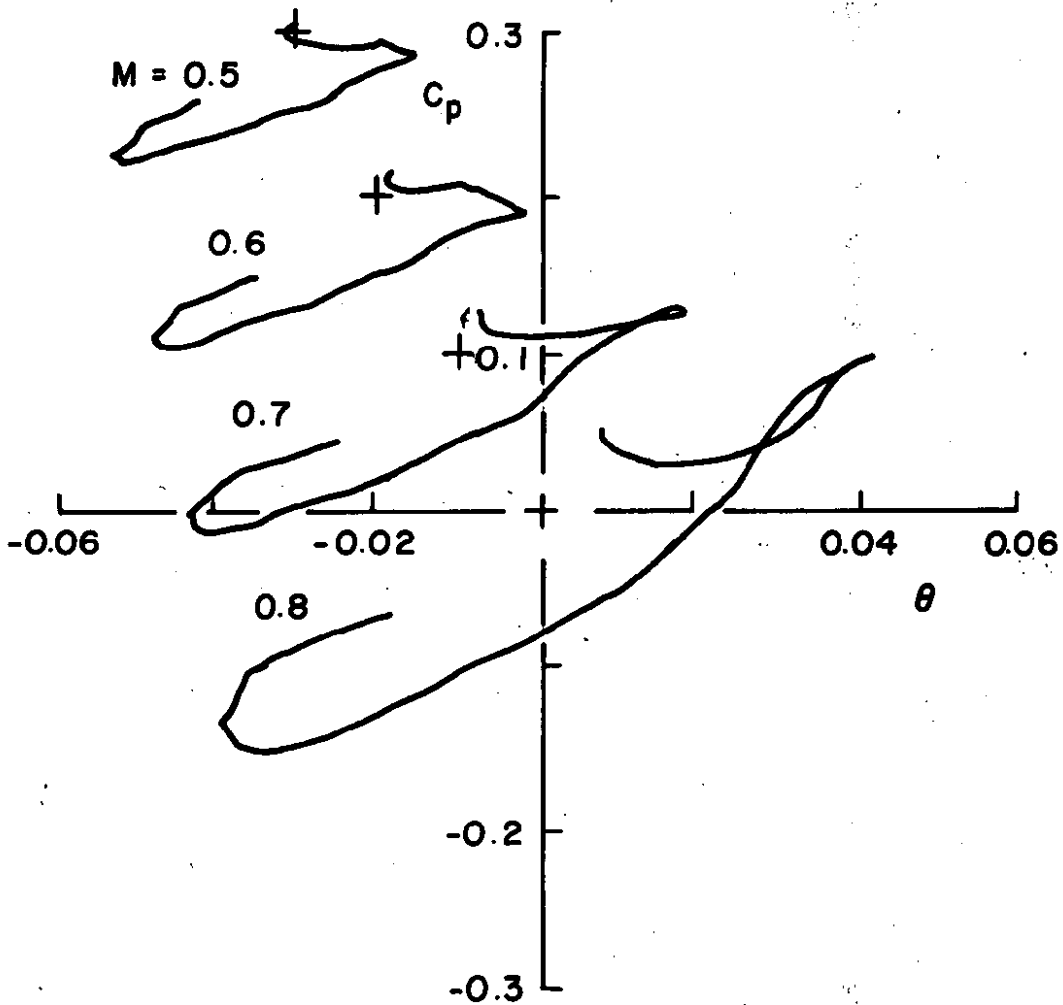
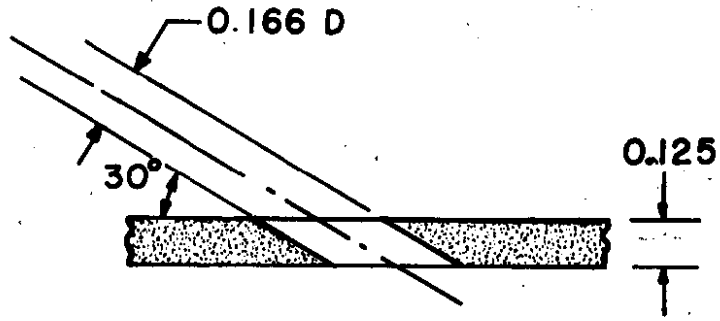
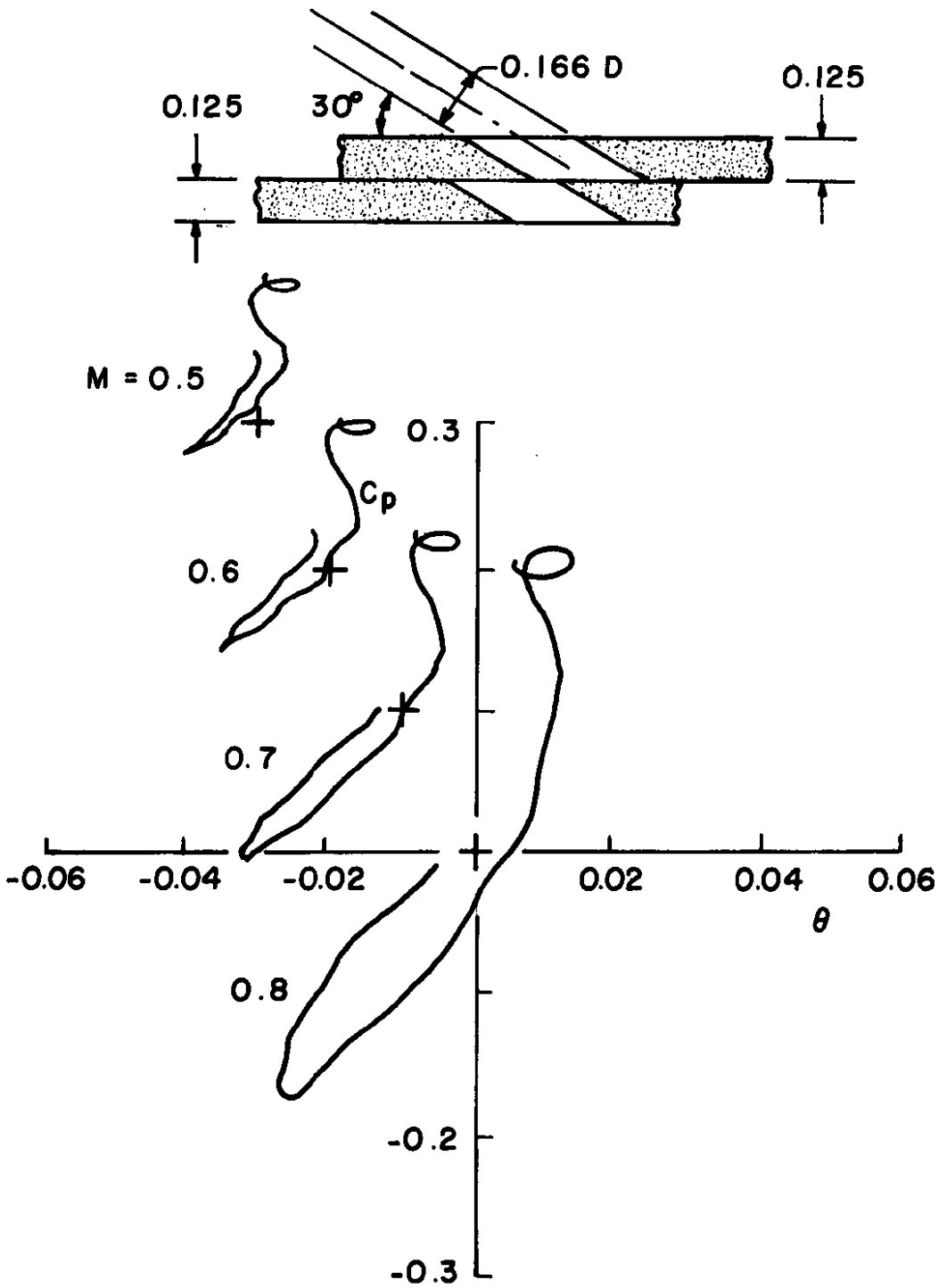
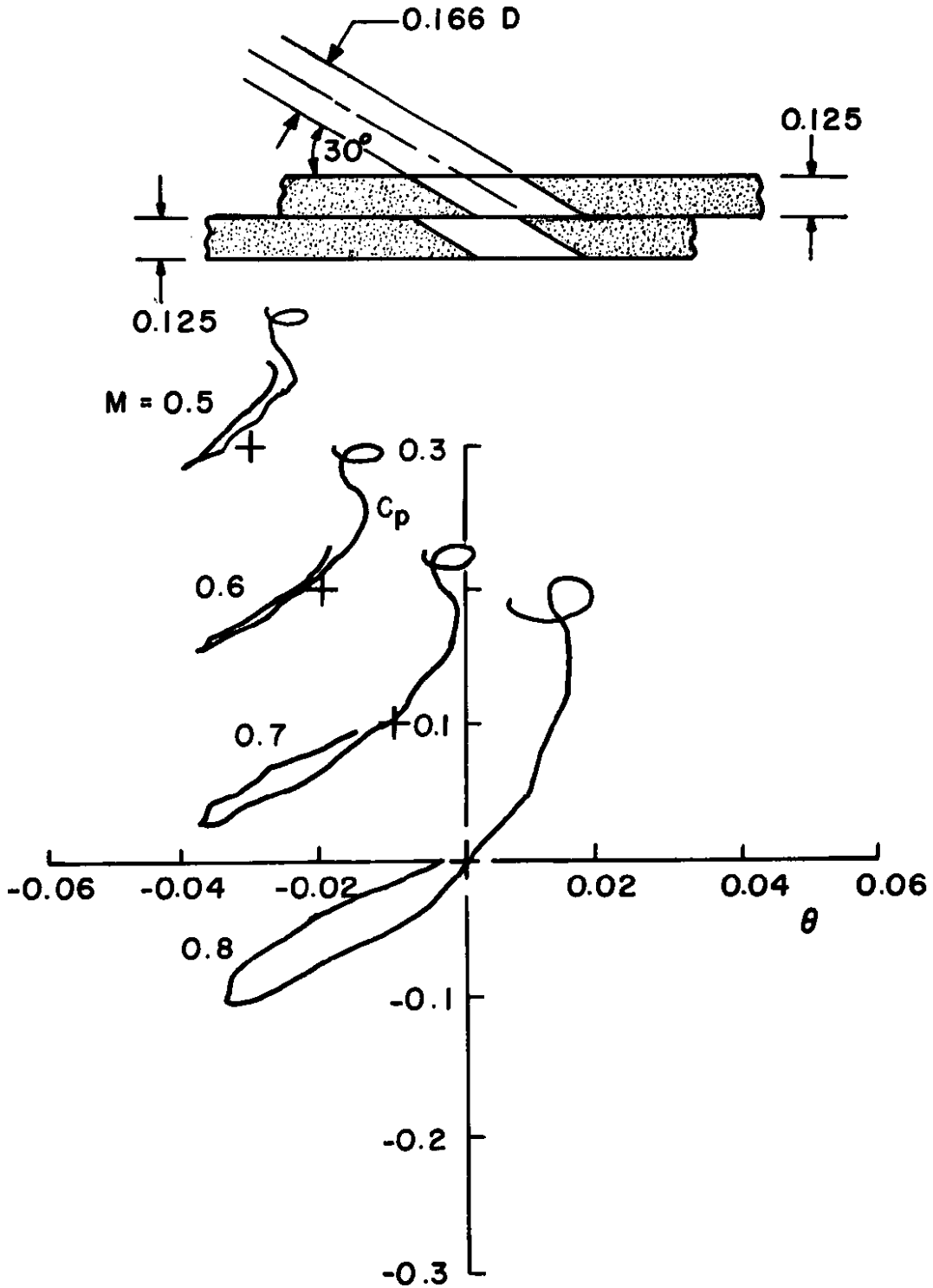


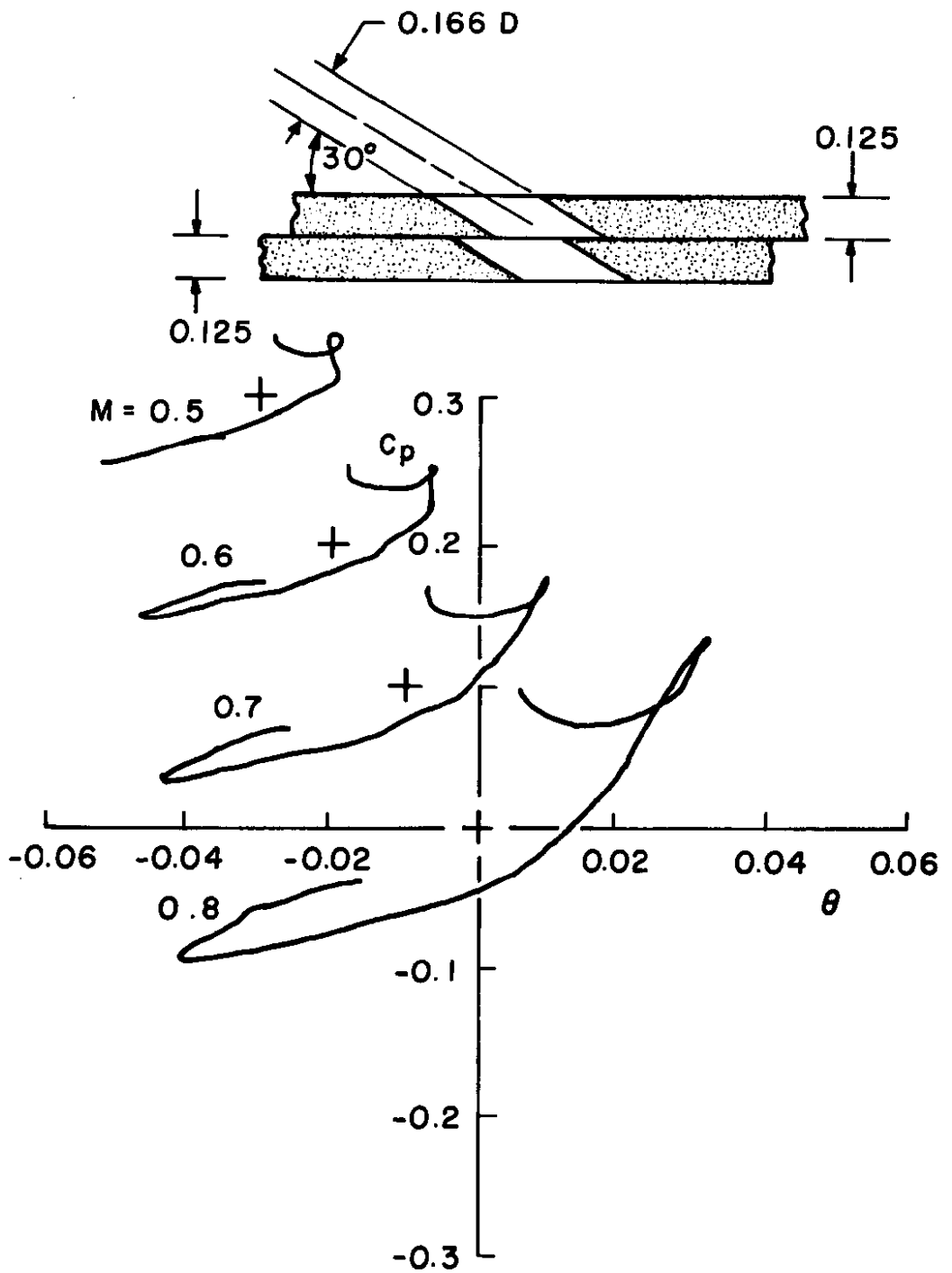
Figure A-3. Characteristics of configuration C10.0.



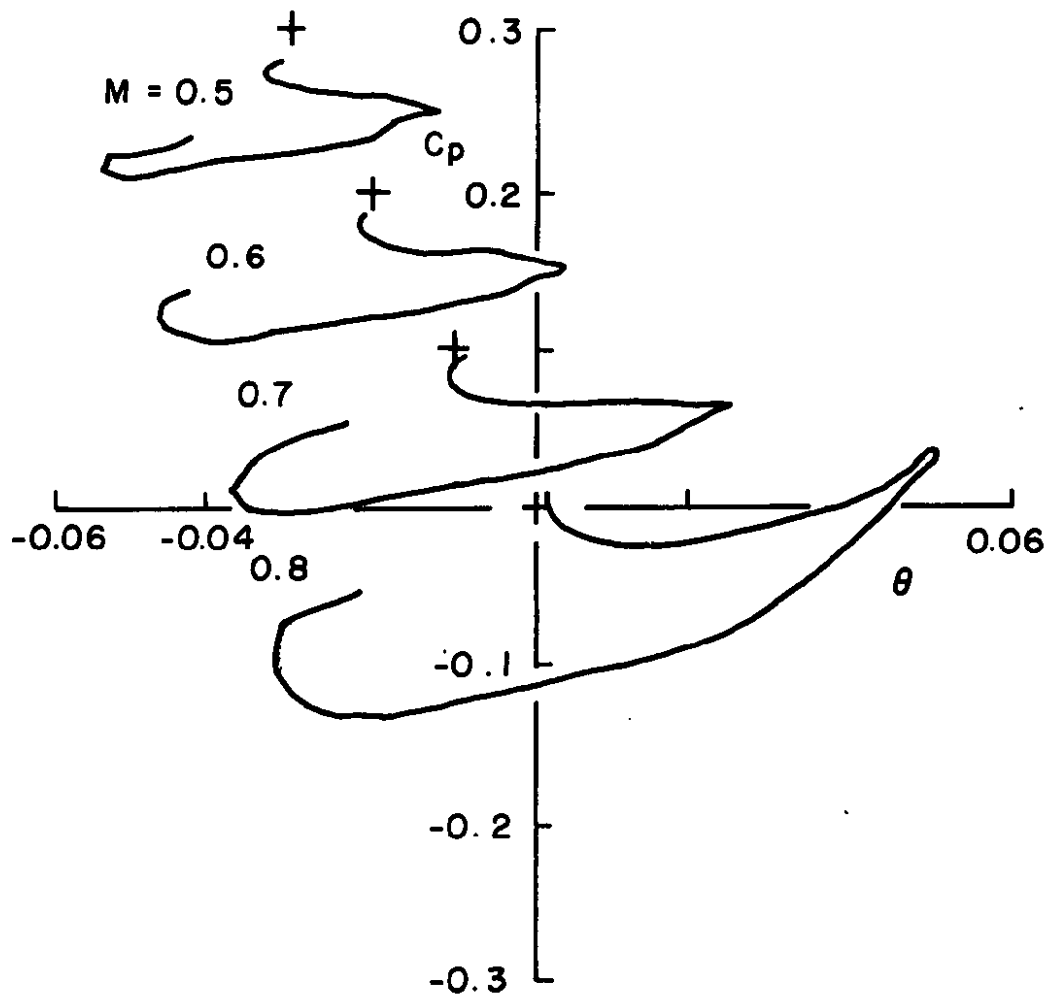
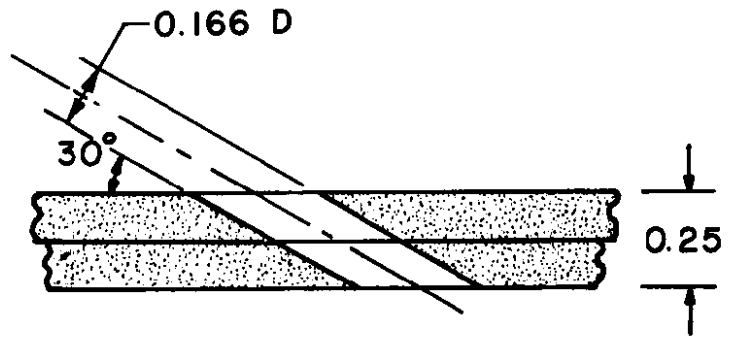
a.  $\tau = 1.0$  (upstream)  
 Figure A-4. Characteristics of configuration D.



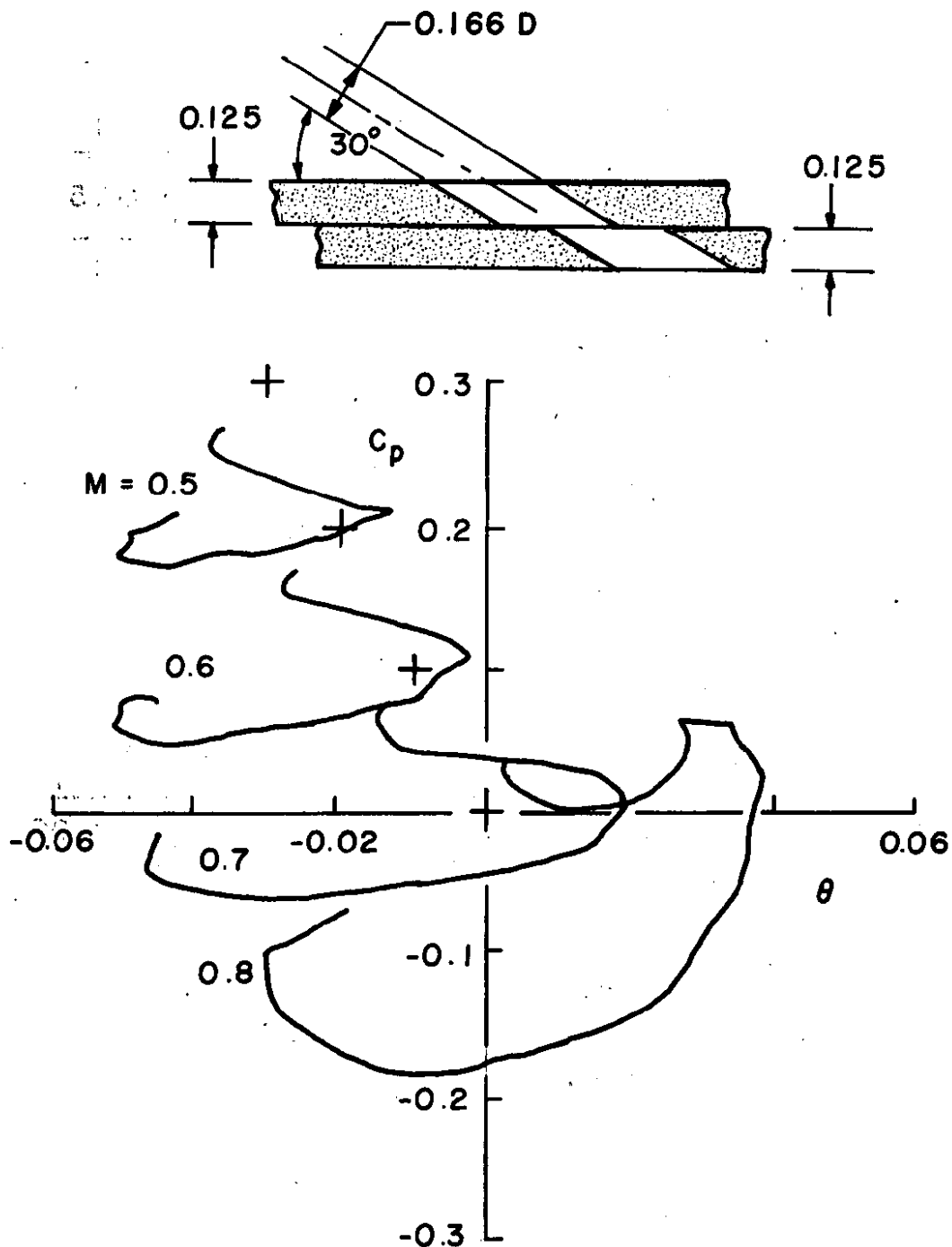
b.  $\tau = 2.5$  (upstream)  
Figure A-4. Continued.



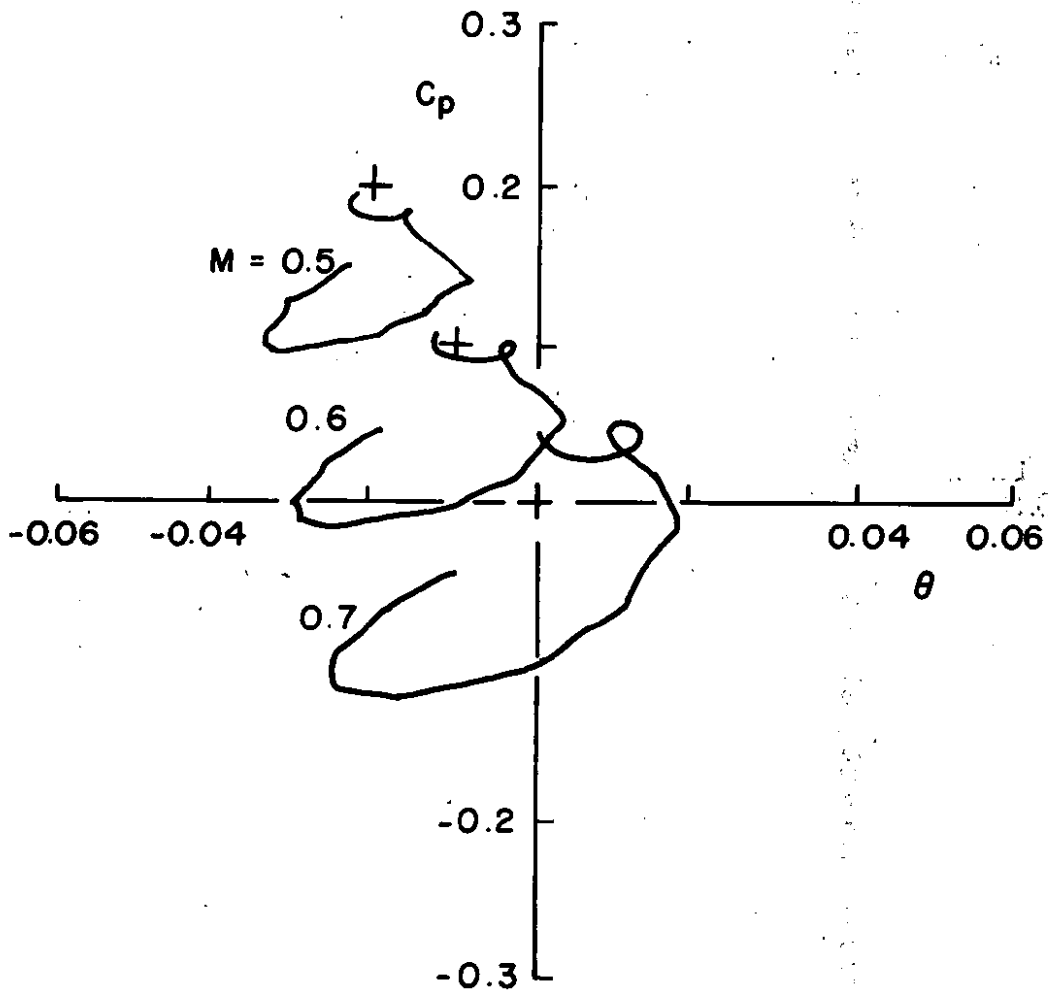
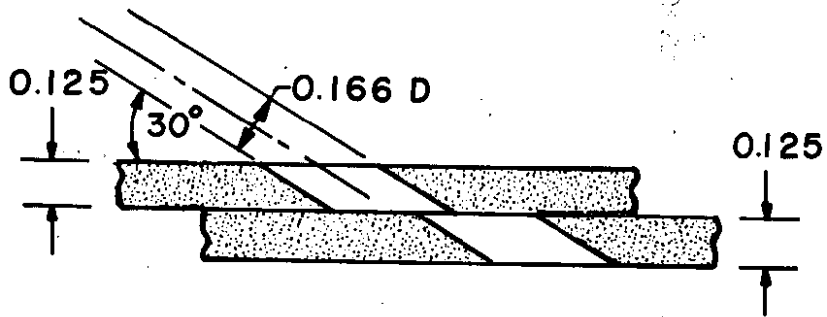
c.  $\tau = 5.0$  (upstream)  
 Figure A-4. Continued.



d.  $\tau = 10.0$   
Figure A-4. Continued.



e.  $\tau = 5.0$  (downstream)  
 Figure A-4. Continued.



f.  $\tau = 2.5$  (downstream)  
 Figure A-4. Concluded.

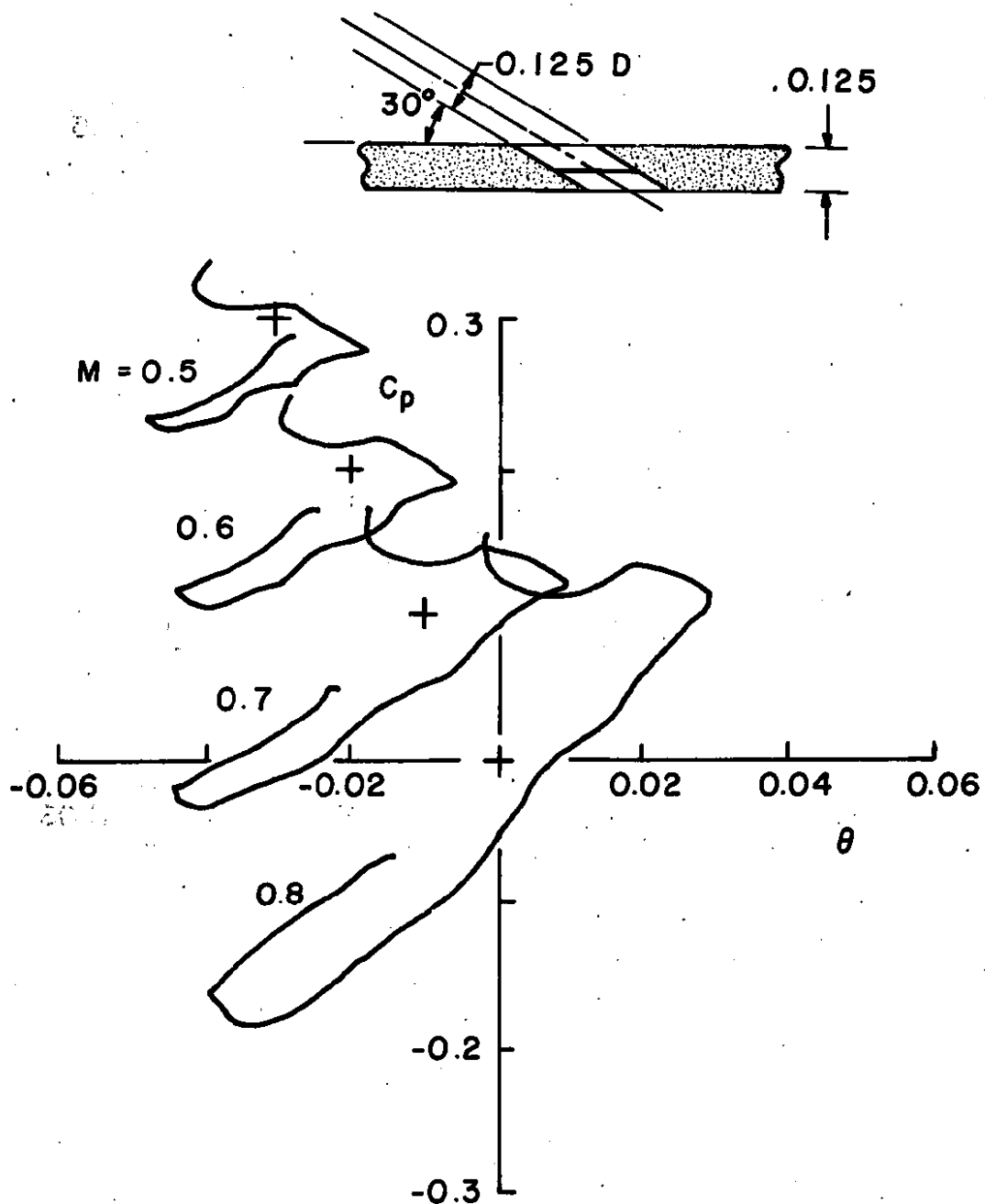


Figure A-5. Characteristics of configuration A6.0 with splitter plates.

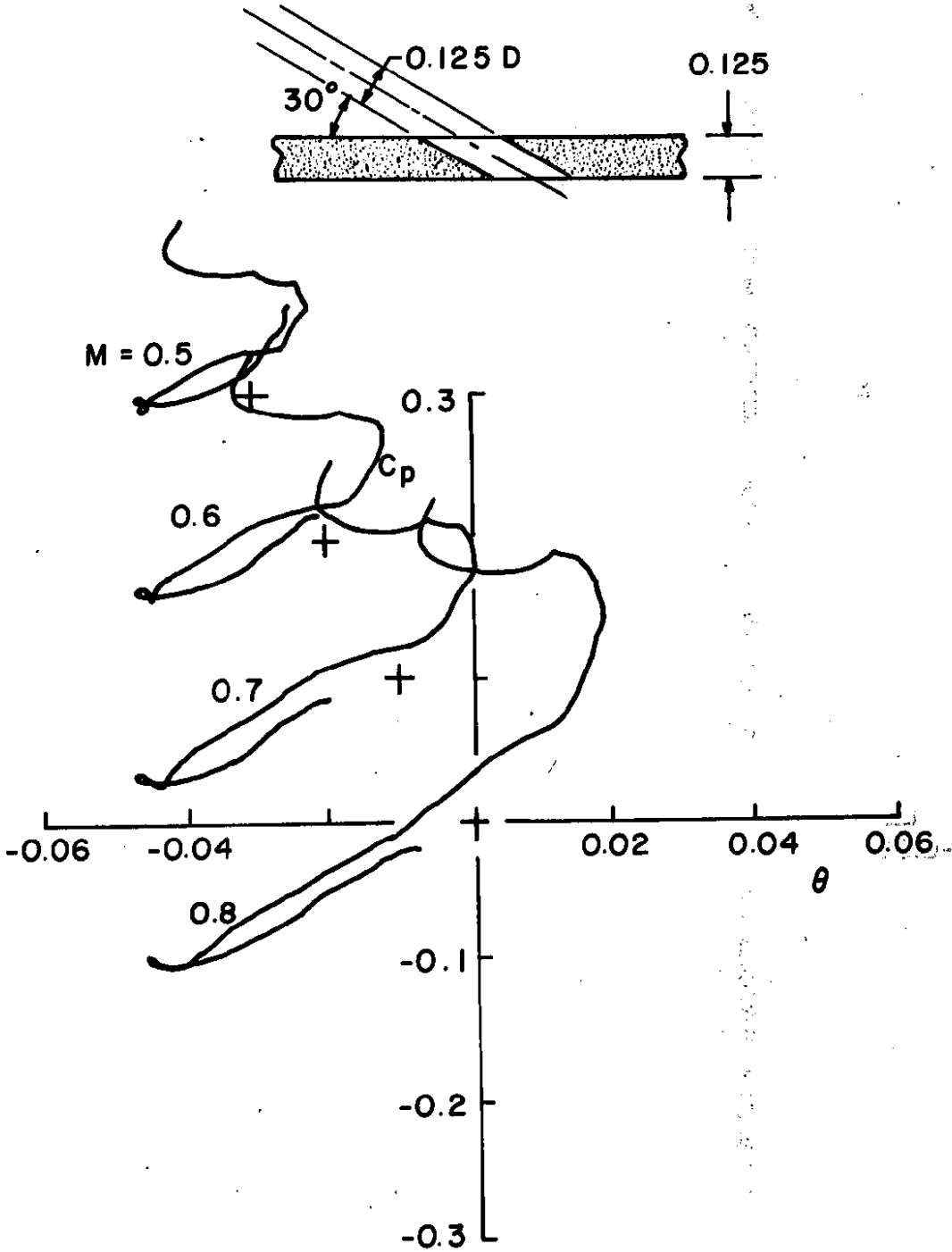
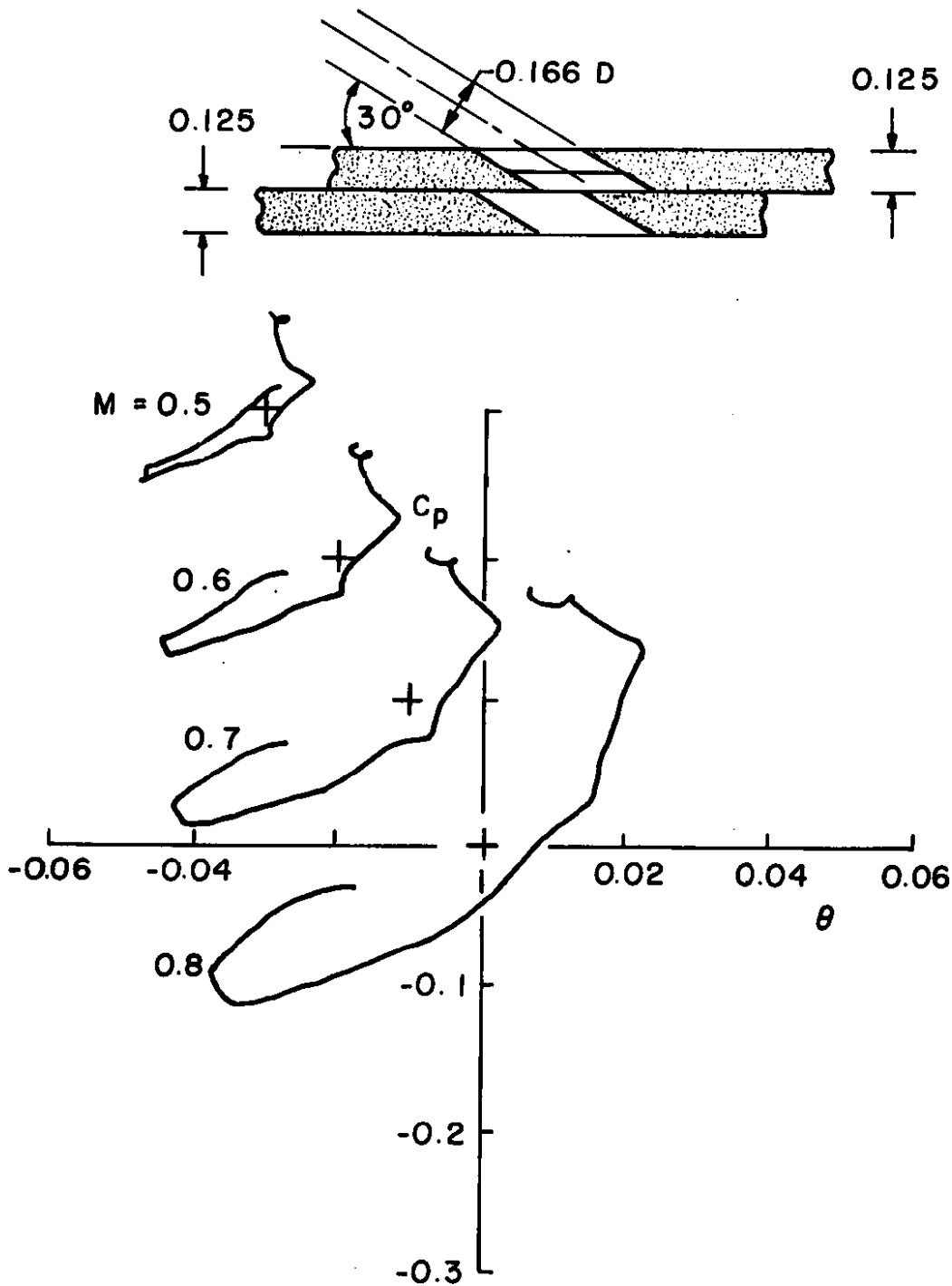
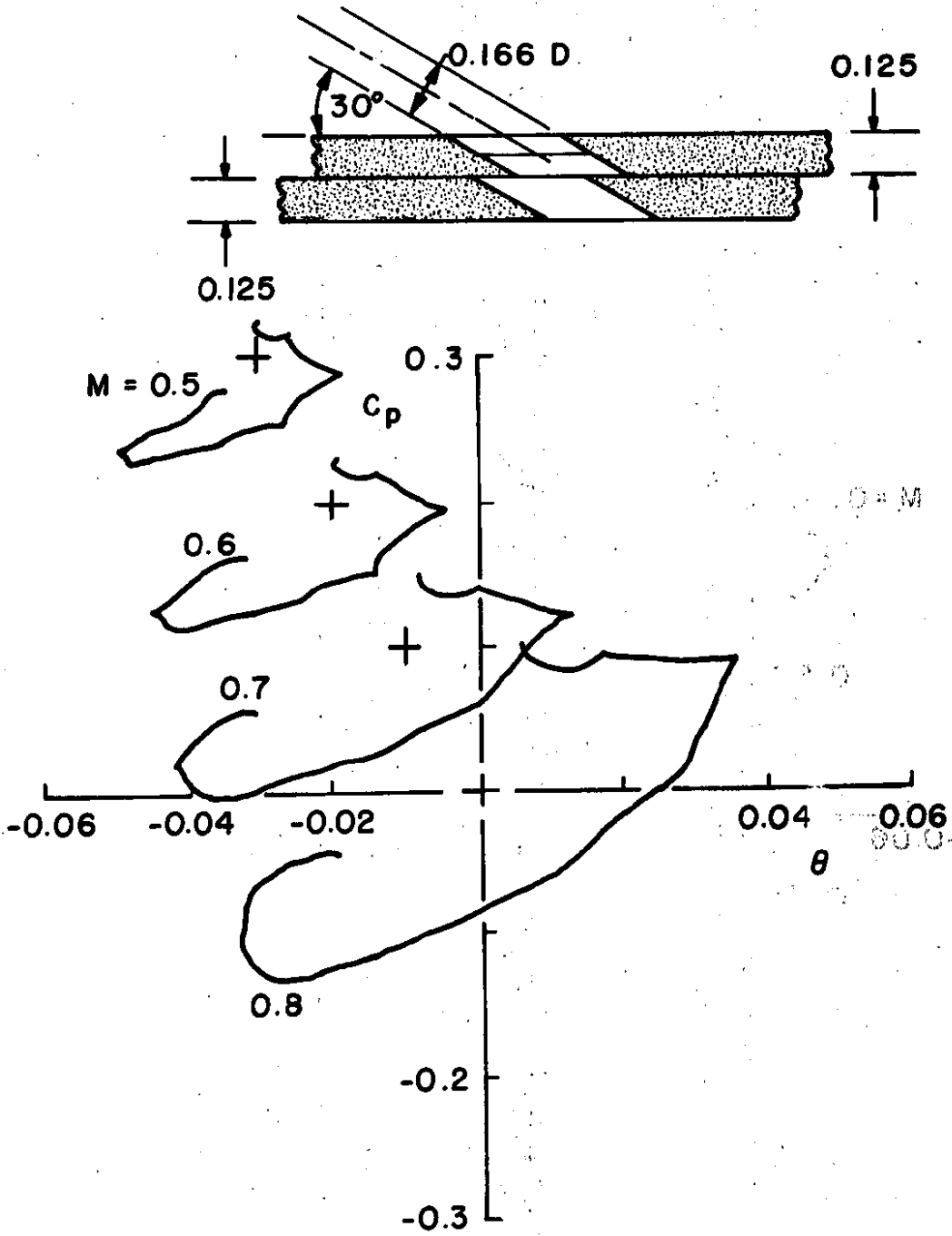


Figure A-6. Characteristics of configuration A6.0 with screen overlay.

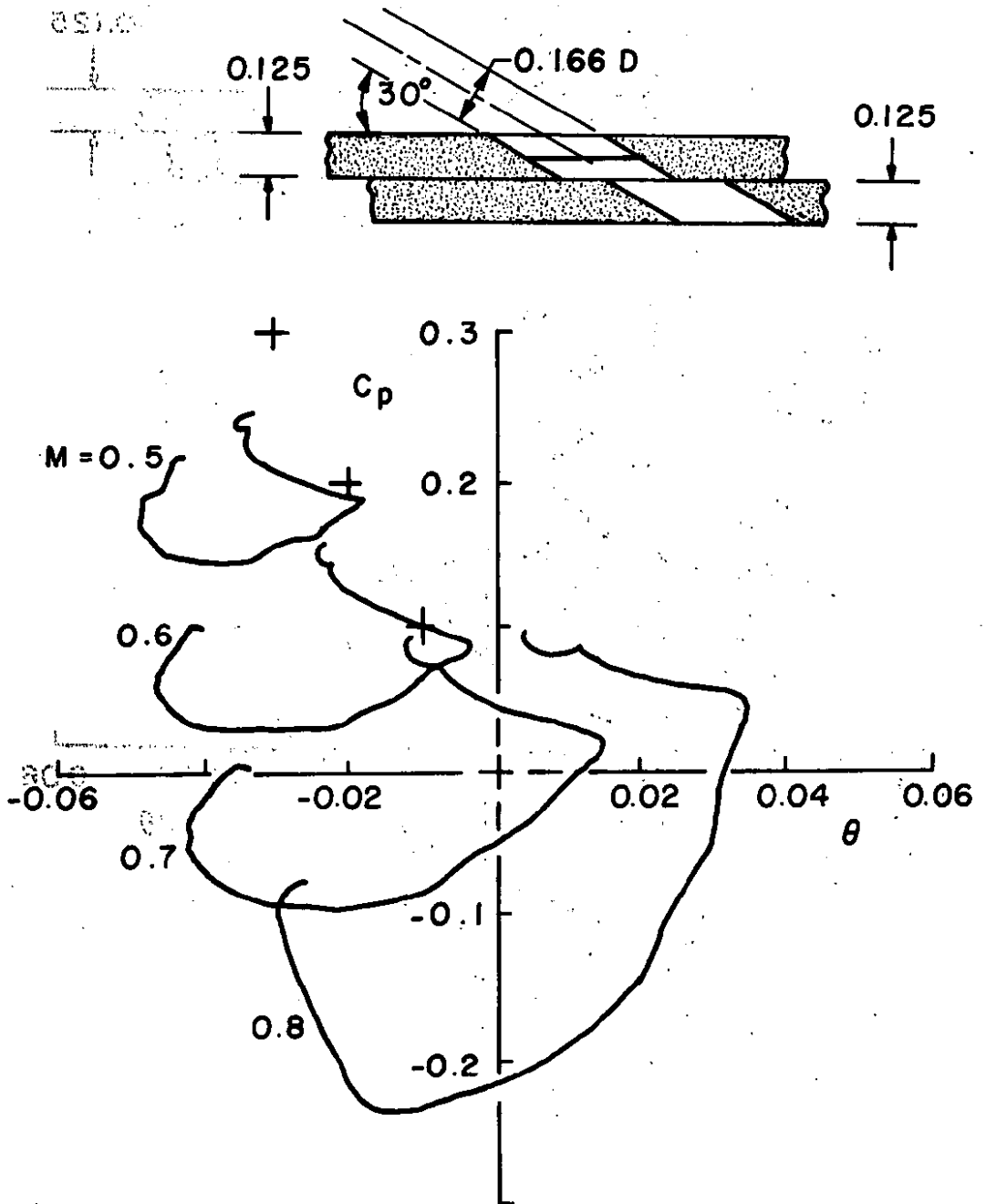


a.  $\tau = 2.5$  (upstream)

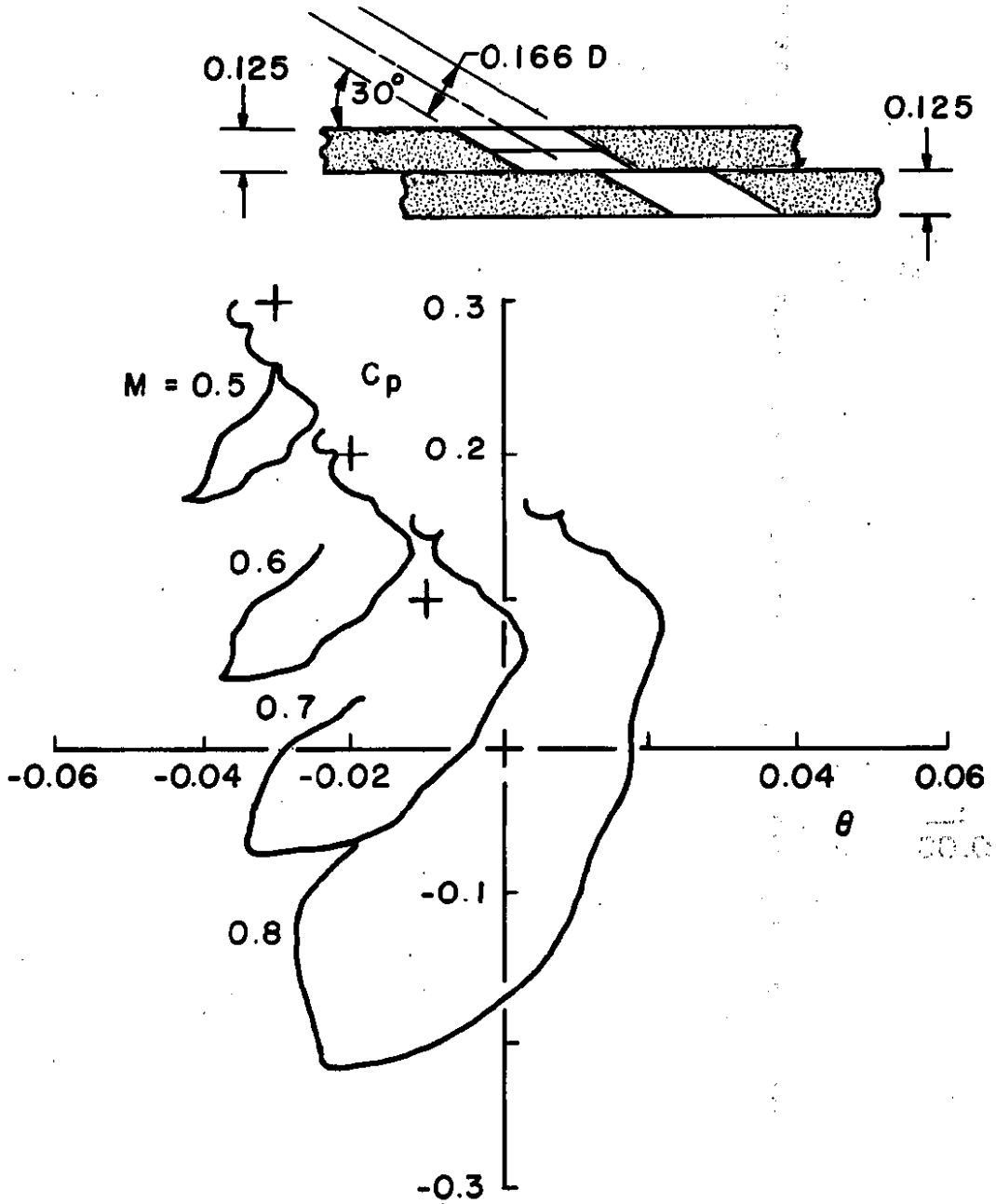
Figure A-7. Characteristics of configuration D with splitter plates.



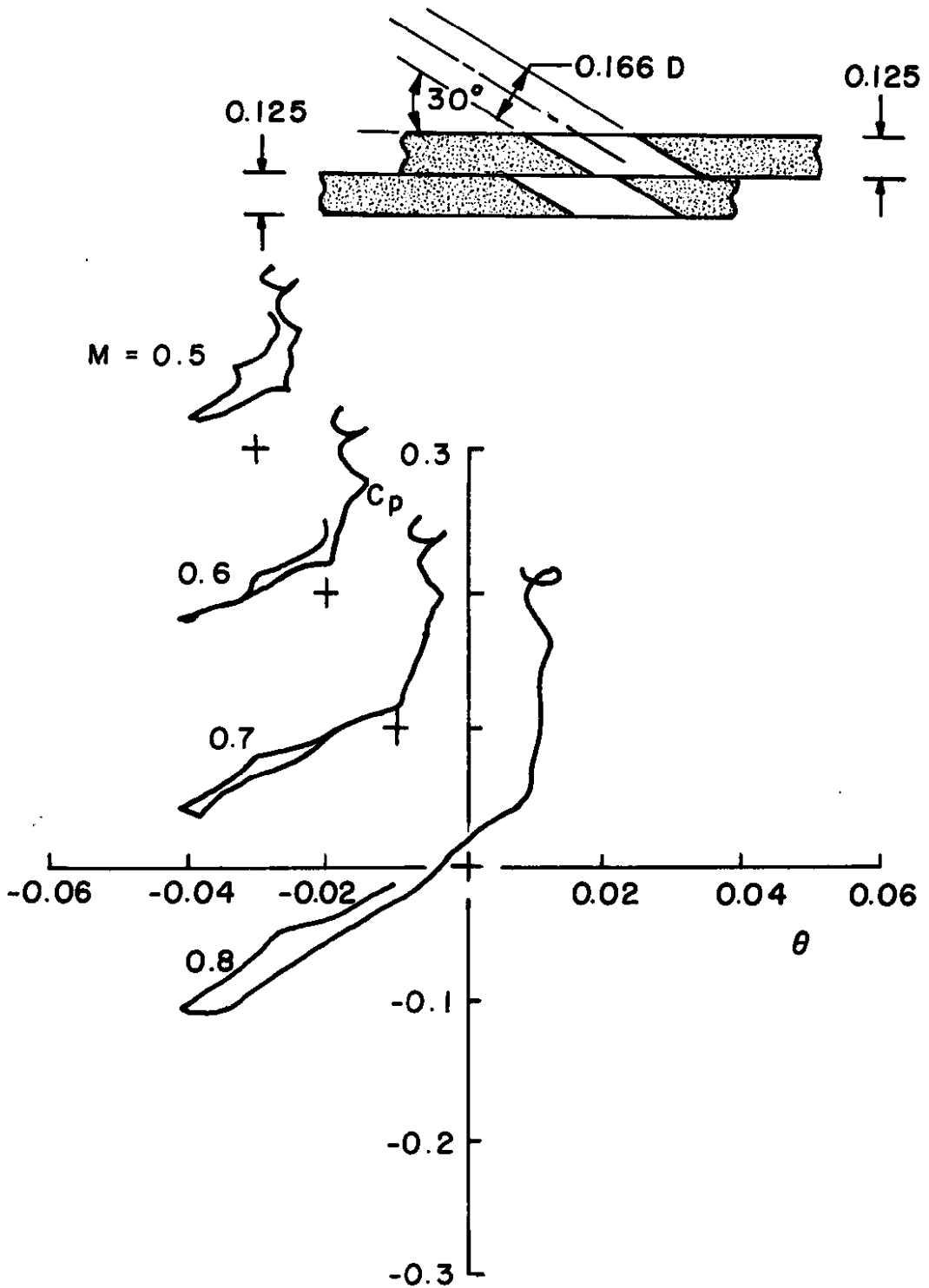
b.  $\tau = 5.0$  (upstream)  
 Figure A-7. Continued.



c.  $\tau = -5.0$  (downstream)  
 Figure A-7. Continued.

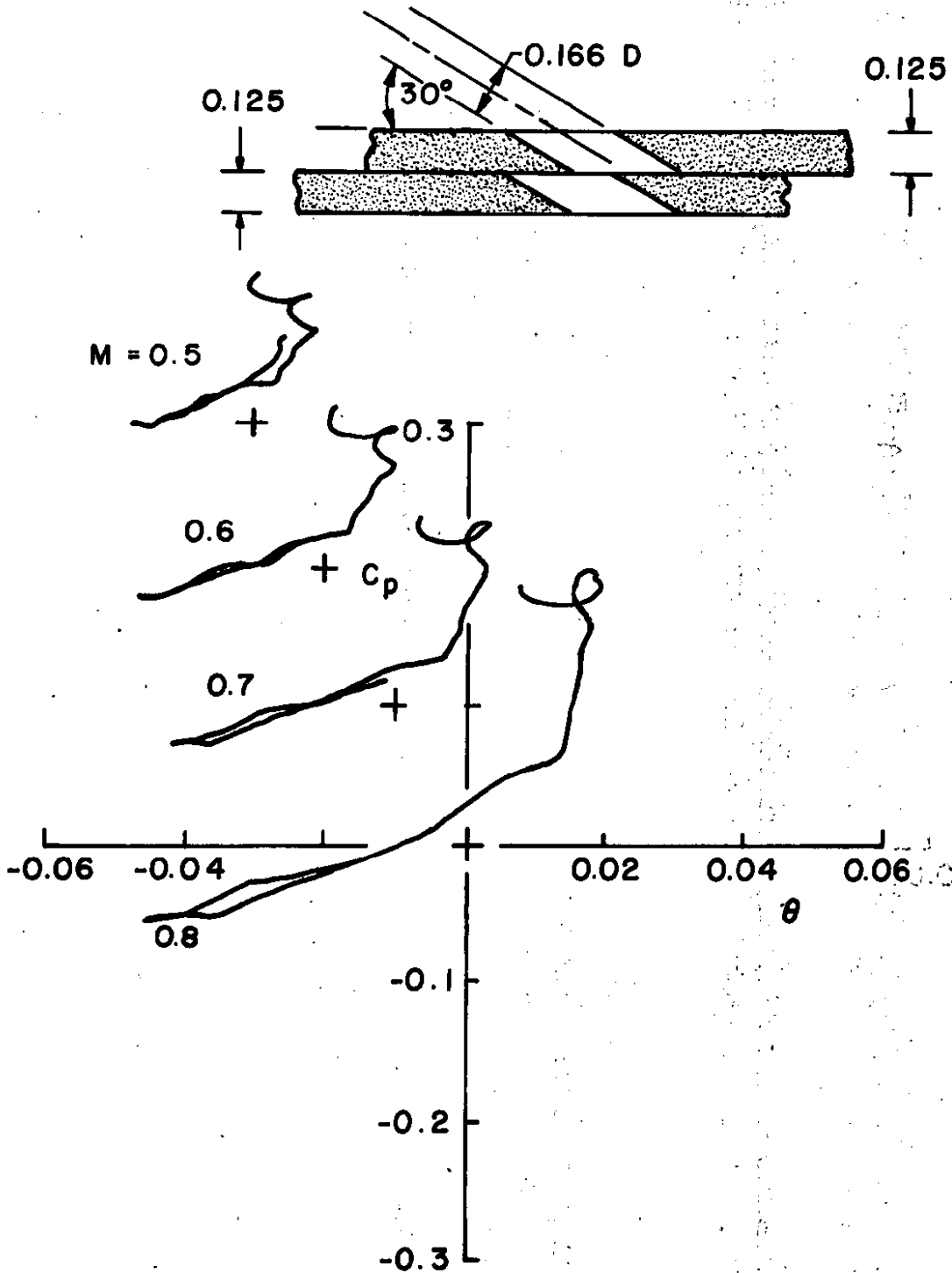


d.  $\tau = -2.5$  (downstream)  
 Figure A-7. Concluded.

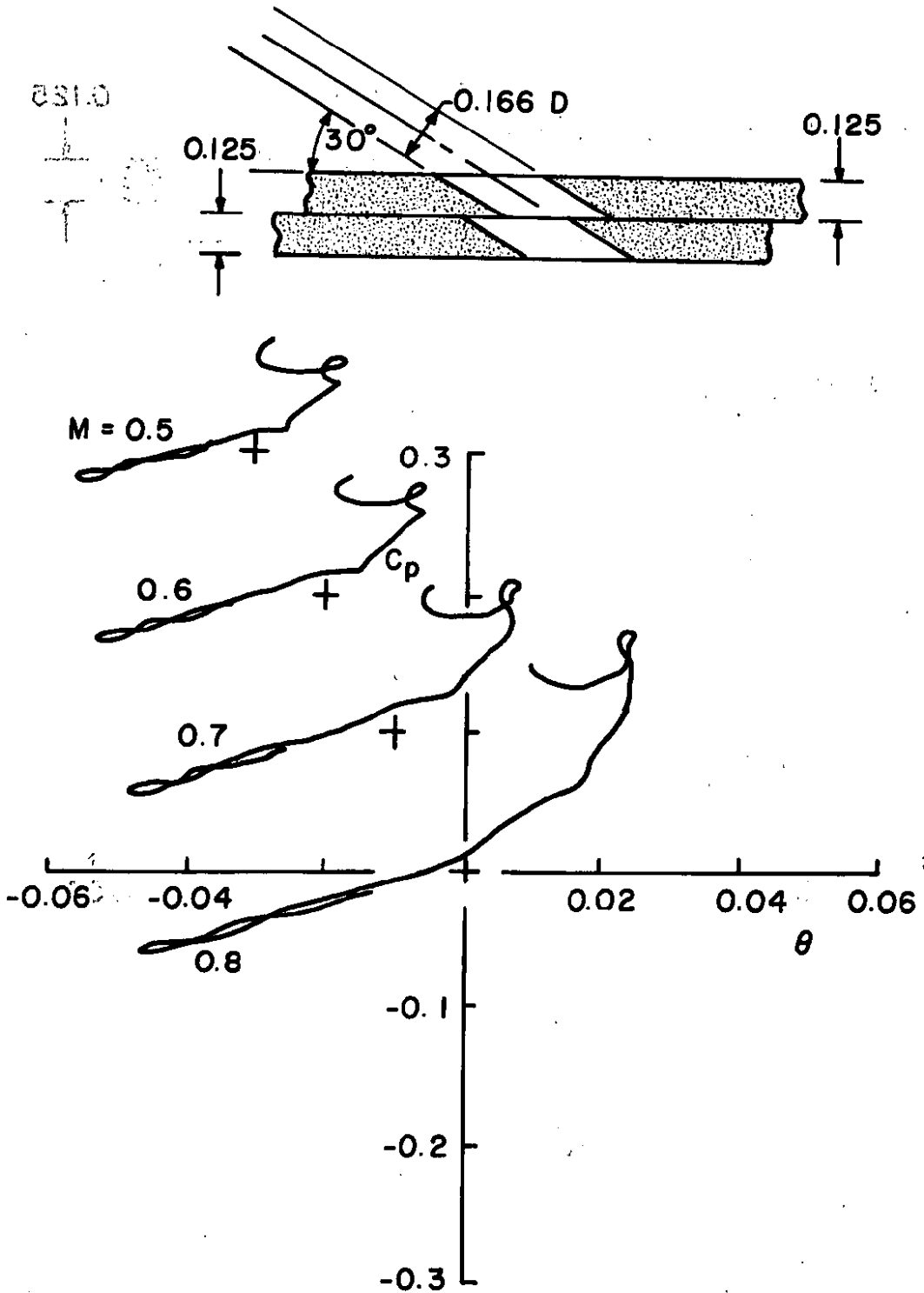


a.  $\tau = 1.0$  (upstream)

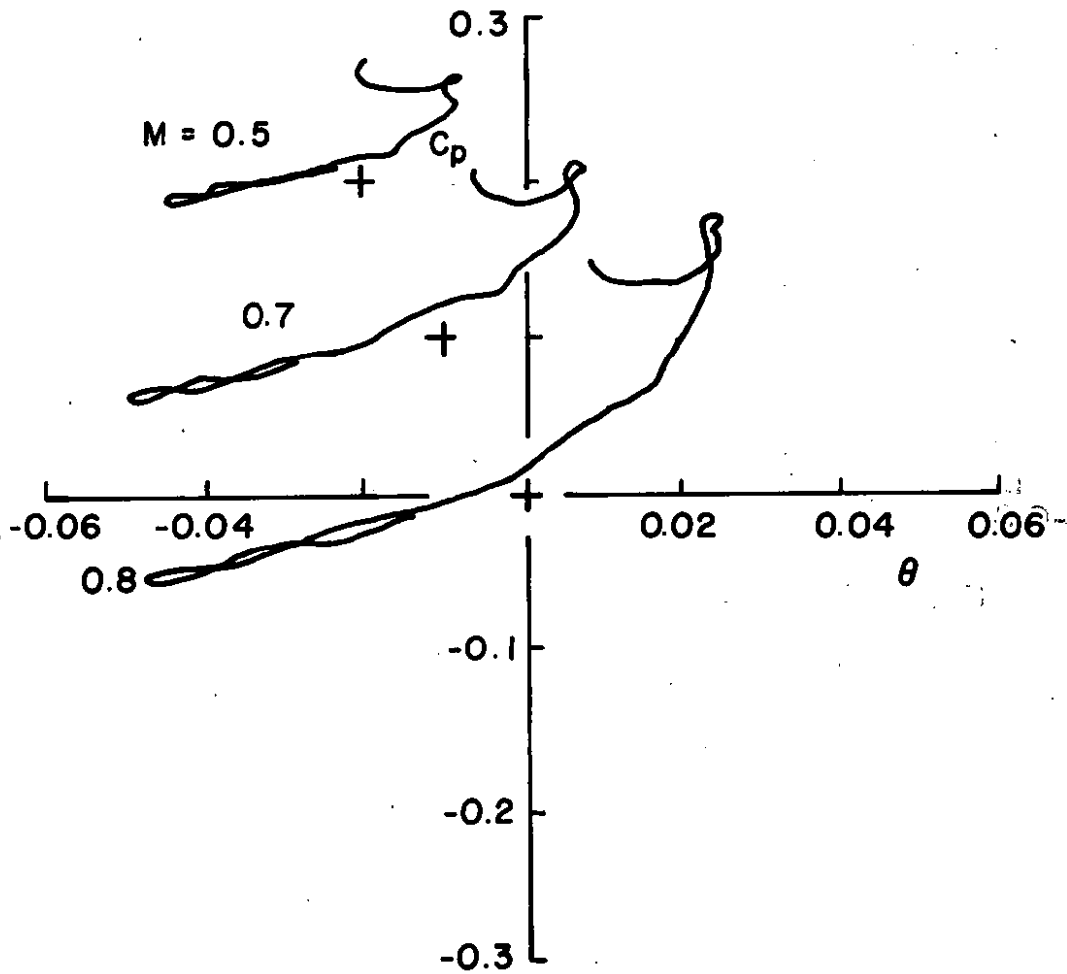
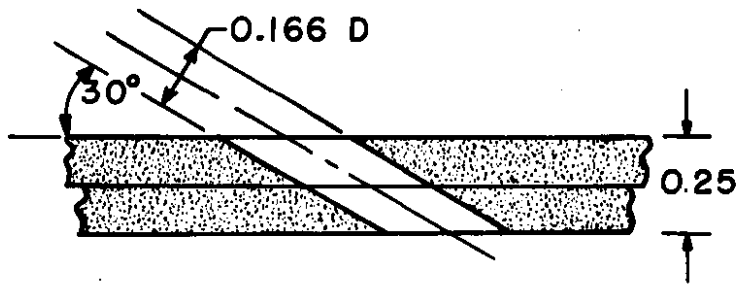
Figure A-8. Characteristics of configuration D with screen overlay.



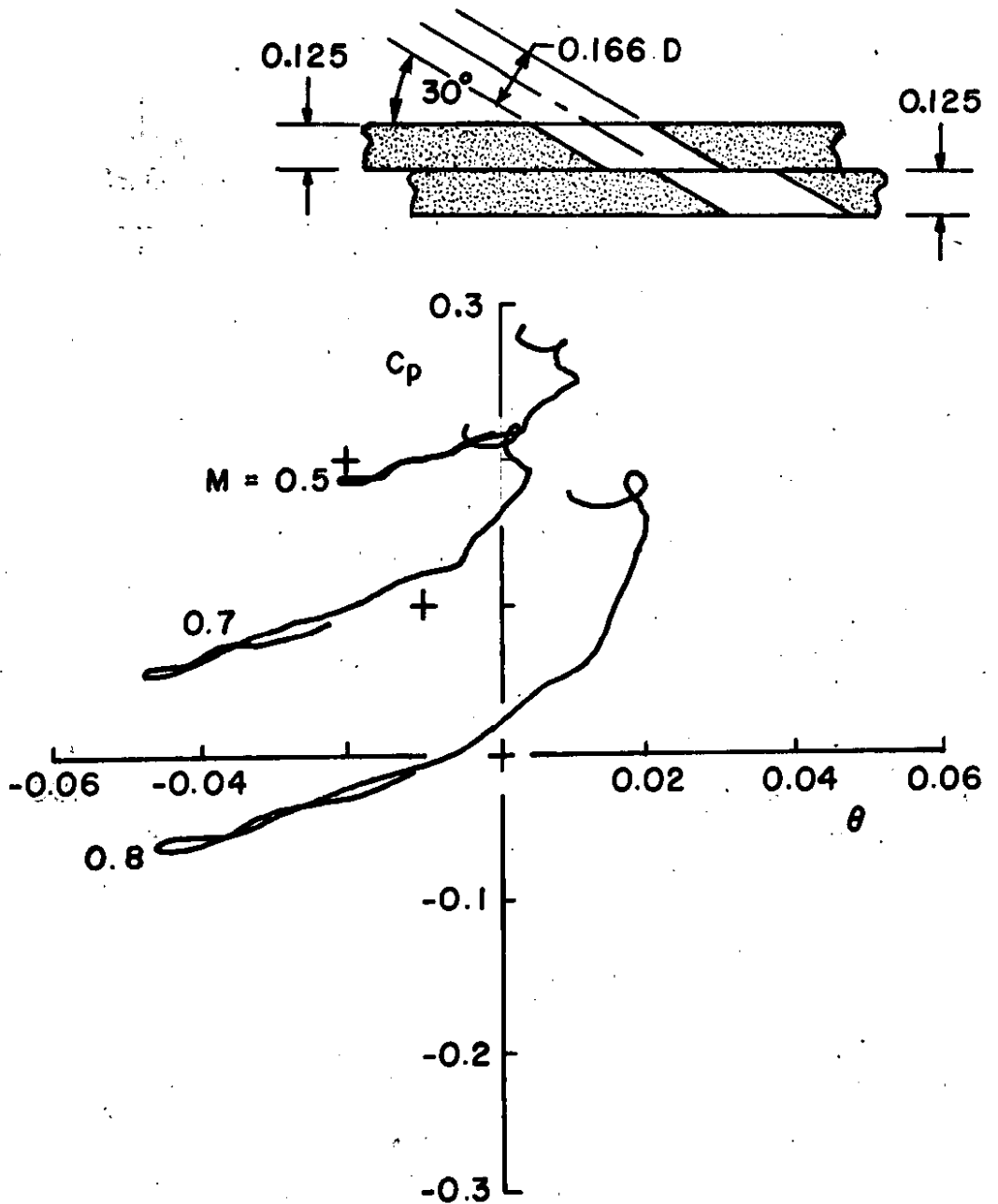
b.  $\tau = 2.5$  (upstream)  
Figure A-8. Continued.



c.  $\tau = 5.0$  (upstream)  
 Figure A-8. Continued.



d.  $\tau = 10.0$   
Figure A-8. Continued.



e.  $\tau = -5.0$  (downstream)  
 Figure A-8. Concluded.

## NOMENCLATURE

$C_f$	Boundary-layer skin-friction coefficient
$C_p$	Pressure coefficient
$d$	Perforated wall hole diameter
$H$	Boundary-layer shape factor, $H = \delta_1/\delta_2$
$h$	Tunnel height
$L$	Tunnel length
$M$	Nominal Mach number
$R$	Wall permeability factor
$t$	Wall thickness
$u_\infty$	Boundary-layer edge velocity
$x$	Streamwise coordinate
$y$	Transverse coordinate
$y_g$	Bottom wall geometry
$y_s$	Streamline shape
$\beta$	Prandtl-Glauert factor, $\beta = (1 - M^2)^{1/2}$
$\gamma$	Specific heat ratio, $\gamma = 1.4$

$\delta_1$	Boundary-layer displacement thickness
$\delta_2$	Boundary-layer momentum thickness
$\delta_\infty$	Boundary-layer control-volume height
$\theta$	Flow angle
$\lambda$	Normalized wall mass flux
$\rho_\infty$	Boundary-layer edge density
$\tau$	Wall porosity
$\phi$	Potential function
$\hat{\phi}$	Particular solution for potential function